UNIVERSITÀ
DEGLI STUDI
DI PADOVA

Head Office: Università degli Studi di Padova

DEPARTMENT OF MOLECULAR MEDICINE
Ph.D. COURSE IN: Molecular Medicine
CURRICULUM: Regenerative medicine
XXXVI SERIES

Design of static and dynamic hydrogel platforms for mechanobiology

Coordinator: Ch.ma Prof.ssa Arianna Loregian
Supervisor: Ch.mo Prof. Stefano Piccolo
Co-supervisor: Ch.ma Prof.ssa Giovanna Brusatin

Ph.D. Student: Lorenzo Ulliana

ABSTRACT

Physical cues that cells receive from the extracellular matrix (ECM) are primary drivers of cell and tissue behavior, determining stemness, cell differentiation and proliferation and are often decisive in disease development and progresses. In this context, 2D substrates of controllable mechanical properties are indispensable tools for mechanobiology studies, as they allow to recapitulate biophysical and adhesive cues of natural ECM.

In this thesis work I designed and developed tools for cell culture having defined mechanical properties and adhesiveness to study mechanotrasduction events in the context of aging and from a molecular biology perspective. I systematically studied the mechanosignalling properties of these systems, monitoring the activation state of the mechanotrasducers YAP and TAZ for diverse cell types.

I optimized a norbornene-terminated Polyethylene glycol (PEG-NB) based hydrogel, in which stiffnesses were tunable in a range of physiological relevant rigidities. The relevance of these gels is that the physical stimuli of the substrate could be dissected, in particular rigidity from adhesiveness, allowing to separately study their influence on cell behavior. Using the level of localization of YAP/TAZ mechanotrasducers as a beacon to investigate cell responses and human osteosarcoma U2OS cell line as a paradigm, we found that rigidity is an overarching parameter that regulate cell mechanotrasduction. However, at intermediate physiologically relevant stiffness (<1-few kPa), adhesiveness can impair stiffness. Moreover, a threshold of 150 μm^2 nuclear projected area is a necessary checkpoint to be surpassed for YAP/TAZ activation.

Using polyacrylamide based gels, I developed substrates with different fixed stiffnesses, finely tunable in a broad range of physiological relevant rigidities (static gels), that could also be decreased in time during cell culture (dynamic substrates), without the need of detach cells from the culture substrate. These tools allowed to mimic the dynamic processes occurring in natural ECM, in particular in the context of tissue aging. Using WI38 fibroblasts, it was found that YAP/TAZ activity is impaired in ECM typical of aged tissues. Studying this phenomenon both in vivo and in vitro, we found that YAP/TAZ mechano-activation induced tissue senescence, demonstrating that these aging traits are due to cGAS-STING activation and consequent inflammation processes. Indeed, by YAP/TAZ rescue these processes are inhibited.

Finally, to fully recapitulate the dynamicity of the ECM I optimized substrates that undergo to a periodical deformation during cell culture, by means of a stretching device. Studies of cell responses to periodical mechanical cues are on-going. Preliminary results show that YAP/TAZ activity is instrumental in preserving nuclear envelope integrity from damage arising from repeated, acute

mechanical strains, as such providing a protection mechanism from the onset of an ageing-associated inflammatory phenotype in fibroblasts.

PUBLICATIONS

1 Gandin, A., Murugesan, Y., Torresan, V., Ulliana, L., Citron, A., Contessotto, P., Battilana, G., Panciera, T., Ventre, M., Netti, A. P., Nicola, L., Piccolo, S., Brusatin, G. "Simple yet effective methods to probe hydrogel stiffness for mechanobiology." Scientific Reports 11.1 (2021): 22668.
https://doi.org:10.1038/s41598-021-01036-5

2 Gandin, A., Torresan, V., Ulliana, L., Panciera, T., Contessotto P., Citron, A., Zanconato, F., Cordenonsi, M., Piccolo, S., Brusatin, G. "Broadly Applicable Hydrogel Fabrication Procedures Guided by YAP/TAZ-Activity Reveal Stiffness, Adhesiveness, and Nuclear Projected Area as Checkpoints for Mechanosensing." Adv Healthc Mater 11, e2102276 (2022).
https://doi.org:10.1002/adhm.202102276

3 Sladitschek-Martens, H. L, Guarnieri, A., Brumana, G., Zanconato, F., Battilana, G., Xiccato, R. L., Panciera, T., Forcato, M., Bicciato, S., Guzzardo, V., Fassan, M., Ulliana, L., Gandin, A., Tripodo, C., Foiani, M., Brusatin, G., Cordenonsi, M. & Piccolo, S. "YAP/TAZ activity in stromal cells prevents ageing by controlling cGAS-STING". Nature 607, 790-798 (2022).
https://doi.org:10.1038/s41586-022-04924-6

Table of Contents

INTRODUCTION

Biomaterials are instrumental in exemplifying the role that physical stimuli have in shaping cell behavior, i.e. cell mechanobiology. Since the beginnings of the field[1], biomaterial platforms enabled seminal discoveries, such as the relation between cell shape and cell behavior (proliferation, differentiation, apoptosis[2]) using micropatterns and the effect of substrate stiffness in cell spreading, migration[3] and differentiation[4].

Still, a major part of established knowledge of cell biology is based on culture techniques that employ supraphysiologically stiff substrates, such as glass and plastic, with elastic moduli in the GPa order of magnitude[5]. These materials fail to reproduce salient features that cell experience in the tissue microenvironment, and in particular the range of mechanical properties characteristic of various soft tissue (as quantified by elastic moduli E under 1 kPa for brain and approaching 15 kPa for muscle tissues)[6].

Mechanobiology

Cells are responsive to multiple kinds of signals from the environment: soluble molecules (mitogens, morphogens), spatial organization of insoluble molecules and mechanical stimuli (forces). Studies focusing on key biological phenomena, such as cell differentiation[4], migration[3,7], proliferation and apoptosis[2], have highlighted the centrality of physical cues in directing cell behavior, such as the forces and cell architecture imposed by the local microenvironment[8].

Indeed, cells can read the forces originating from their surroundings (mechanosensing) and convert the information into biological activity (mechanotransduction). The complex mechanisms allowing these processes are essential for maintaining tissue development, repair and homeostasis.

Cells respond to diverse mechanical inputs : changes in composition and size of substrate adhesions, cytoskeletal structure and tension, and activation of transcriptional programs[9].

Alterations in any of the elements of this complex system (such as tissue stiffening in fibrosis[10], or mutations in the gene expression of mechanically relevant proteins such as lamins[11]) can lead to the initiation and progress of severe diseases such as cancer and dystrophies, and explain aging and some aging related diseases. Thus, advancing research in the field of mechanobiology holds great promise to provide insights for disease studies, therapeutics and tissue regeneration.

In this landscape, biomaterials play multiple crucial roles offering cell environments with defined and controllable physical cues (spatial confinement, force transmission, viscoelasticity). Therefore, the possibility of applying physical cues on cells enables in vitro studies of mechanobiology and to build

models for disease studies, but also platforms to instruct cell behavior, for tissue engineering and material-based therapies[12].

The development of biomaterials is an interdisciplinary effort, that requires profound knowledge of how cells interact with their microenvironments, in order to design and tailor the features of the biomaterials, but that cannot prescind taking into consideration the central role of the mechanosensory elements of the cell and how they engage the cell surroundings.

The ECM

A major fraction of cells in the body are adherent, relying on connections to a supporting structure and other cells to survive and form a tissue. The extracellular matrix (ECM) is a three-dimensional network of biomacromolecules, providing such structural support.

Several cell-adhesive proteins, including fibronectin, laminin, collagen provide anchorage points for cells. These adhesion sites are recognized by integrins, specific membrane receptors, capable of discriminating between different proteins and recognizing polypeptide motifs, the most common being the RGD (Arg-Gly-Asp) sequence[13]. As well as binding to the cell surface, glycoproteins also contribute to the organization of the ECM by association with its other components, and present growth factor-binding domains[14].

Three of the main ECM components govern its mechanical properties: fibrillar collagen, elastic fibers, glycosaminoglycans (GAGs) and related proteoglycans[15]. Collagen is the prevalent protein in the ECM of mammals, where is present as multiple types, the most abundant being type I collagen. Fibrous collagen is assembled in a hierarchical structure, its basic building block being a triple helix, and endows tissues with resistance to deformation and failure[14].

Collagen triple helices expose domains that are specifically recognized by integrins, such as the GFOGER sequence[16], but also feature cryptic RGD binding sites, that can be exposed by denaturation or enzymatic degradation, in a process that is deemed relevant in directed migration after tissue injury[17]. Elastic fibers are comprised of core of a rubber-like core network of hydrophobic elastin surrounded by glycoprotein microfibrils (fibrillin, fibulin), that allow extensibility and resilience (recoil after force loading) to the tissue and are most abundant in vascular tissue[14]

GAG are highly hydrated anionic polysaccharide chains, most types of GAGs in the ECM are present in proteoglycans, containing a core protein with multiple covalently attached GAG chains, with the exception of hyaluronan, a nonsulfated linear glycan[18]. Hyaluronan and proteoglycans endow the ECM with water retention, viscosity and compressive resistance: for instance, the highly sulfated aggrecan is the major load bearing component in cartilage tissue[19].

The composition and structure of the ECM are dependent on the specific tissue, and subject to changes during development, disease and aging. Examples include stiffening following injury[20], fibrosis and tumor progression[21], and remodeling of the matrix involved in cell migration, wound healing and tissue development[22].

Cell activity is instrumental in ECM maintenance and remodeling, through deposition of matrix components and production of enzymes that crosslink or degrade them, but also through the exertion of forces: physiological processes are guided by the dynamic reciprocal interactions between cells and the ECM[15]. For instance, In tumors, fibroblasts are induced into in a contractile and matrix-deposing phenotype (Cancer Associated Fibroblasts, CAF)[23] provoking collagen reorganization and crosslinking, involved in tissue stiffening that characterizes cancer progression[21].

Integrin-based adhesions

Integrins are regarded as the main receptors relaying signals between the ECM and the cell: they are type I transmembrane proteins, expressed on the cell surface as obligate, non-covalent heterodimers (subtypes) of α-subunits and β-subunits, and are able to respond to fundamental cues such as rigidity and topography of the ECM and externally applied forces. Their role in mechanosensing is supported by diverse force-controlled behaviors, such as conformational changes (from a bent, low affinity conformation to an extended, high affinity one)[24], force sensitive (catch/slip) bonds with ECM ligands and clustering[25].

Cells usually express multiple integrin subtypes, that recognize specific sequences in adhesive proteins[26] and possess different responses of the bond to force[27-29].

Integrins are not evenly distributed on the cell surface, rather, they form aggregates of different molecular composition, size and shape (IAC, integrin adhesion complexes). The assembly and development of these complex structures is guided by intracellular signaling and the type and spatial distribution of available ligands provided by the ECM[30], but is also dependent on local mechanical forces, either applied from inside or outside of the cell[31,32].

IACs are reliant on interactions with many other proteins to enable and modulate their functions. For example, on the cytoplasm side, IACs recruit scaffolding and signaling proteins: mature adhesions are identified by the increase in size and elongation, and by the enrichment of actin-binding proteins such as vinculin, talin, zyxin, a-actinin and tyrosine-phosphorylated focal adhesion kinase (FAK)[25,33-35]. FAK constitutes a key signaling center of the adhesion, for instance it associates with both promoters and inhibitors of small GTPases, thus regulating cytoskeletal structures and contractility[36]. On the

membrane side, integrins cooperate with syndecan transmembrane proteoglycans to form adhesions, an interaction that is also involved in cytoskeletal control through the regulation of Rac1 and RhoA[37].
While nascent adhesion/focal complexes (<100 nm in diameter) form irrespectively of force and substrate rigidity[38,39], if sufficient adhesions motifs are available and tension is established, they can develop into larger focal adhesions (FA) linked to contractile actin stress fibers through adaptor proteins[25]. When cell traction is inhibited, focal adhesions decrease in size[40], adaptor proteins and FAK disassociate[41] leading to disassembly.
Cells can also adhere to substrates that do not specifically engage integrins, such as poly-L-lysine (PLL) or concavalin A. However this greatly limits cell spreading[42,43] and does not support the maturation of focal adhesions[44,45], notably, these non-specific interactions can enforce attachment to a substrate on cell types that would be otherwise non-adherent[46,47].
Processes like cell spreading, involving adhesion turnover, and cell migration, requiring the disassembly of adhesions located at the cell rear, are dependent on coordinated dissociation of IACs: the control of this process has been shown to be mediated by microtubules, and depends on FAK and dynamin[48] (endocytosis) and dynesin[49] (delivery of signals to target adhesions), and involves the activity of the calcium dependent protease calpain[50].
A study employing FRET tension sensors has evidenced how vinculin recruitment and force transmission are independently controlled, and that a low force across vinculin mediated adhesion disassembly[43]. While focal adhesions have been mainly studied by observing cells on 2D substrates, analogous molecular structures have been observed in 3D matrices for cells displaying mesenchymal migration, such as fibroblast (as opposed to amoeboid cells, such as lymphocytes and dendritic cells, that do not present developed focal adhesions)[51].

The cytoskeleton

The cytoskeleton plays a central role in determining cell shape, organization and mechanics: it is a network of fibrous protein polymers that can dynamically assemble and disassemble in response to forces[52]. The cytoskeleton contains three main types of filaments: actin microfilaments, microtubules and intermediate filaments.
Beyond being passive structural elements of the cell, stress fibers (SF), bundles of crosslinked actin fibers, can act as tension-generating elements by actomyosin contraction and are instrumental for mechanosensing[53].

Through live cell imaging exploiting fluorescently tagged actin[54], and the actin binding peptide LifeAct[55] it is possible to observe distinct classes of stress fibers and actin filaments, and follow their formation and disassembly in response to disruption of other cell components or myosin inactivation. At the cell periphery, highly branched filaments of actin constitute the lamellipodia, a major site of stress fiber and IAC assembly[53,56] dependent on the activity of the actin-nucleating Arp2/3 complex[57]. The main contractile stress fibers are ventral stress fibers and transverse arcs: ventral SF are attached at both ends to the basal membrane of the cell with FA. Transverse arcs are not directly connected to FA, they migrate from the cell edge towards the cell nucleus (retrograde flow) and are connected to dorsal SF, which are anchored to a FA at the distal end, and to transverse arcs at the proximal end, and do not contain myosin II[53].

The actin cytoskeleton has been described as an "active gel": a network capable of tuning its mechanical properties through the amounts of crosslinkers, mainly a-actinin and contractile myosin-II, in response to matrix stiffness, integrating the local mechanoresponse of FA[58]. Indeed, actin fibers and associated proteins are responsive to applied tension, for instance endogenous level of tension, under 20 pN, inhibit spontaneous depolymerization and the activity of actin severing cofilin[15]. In response of tension-induced SF thinning, zyxin is recruited to enhance a-actinin crosslinking[59], and SF respond to stretching-induced severing by bundling[60].

The response to force of the actin cytoskeleton is not limited to single fibers: when plated on soft substratum, mechanosensitive cells such as fibroblasts fail to form a polarized actin cytoskeleton, and instead feature a circular organization, conversely, they form an oriented cytoskeleton on stiff substrates[58,61], similarly, mechanical stimulation by stretching of the substrate induces con induce changes in cytoskeletal rheology and orientation of stress fibers[62].

Along with the role of the force-responsive actomyosin network, microtubules also play a critical role in the regulation of cell mechanics, to the extent that in several cell types experimental microtubule disruption produces enhanced contractility and growth of focal adhesions[63]. A direct mechanical role of microtubules as compression resisting elements has been advanced[64], but also an indirect role mediated by association and delivery of molecules to targeted adhesion sites[65].

YAP/TAZ

YAP (Yes-associated protein) and TAZ (transcriptional co-activator with PDZ-binding motif) are two closely related transcriptional co-activators. YAP/TAZ activity is involved in several fundamental biological processes, such as morphogenesis, tissue regeneration and tumor development[66].

The subcellular localization of YAP/TAZ is a key determinant of their function, as they need to translocate from the cytoplasm to the nucleus in order to activate transcriptional programs that promote cell survival, proliferation, stemness and plasticity[67].

The predominant control mechanism of YAP/TAZ activity is enforced by the substrate mechanics and geometry, and is dependent on the organization and the tensional state of the actin cytoskeleton[68].

Through this regulation, YAP/TAZ function as key mechanotransducers, in fact under low mechanical stimulation, when cells are cultured on soft ECM or on small areas imposing a round cell shape, YAP/TAZ are retained in the cytoplasm and are thus inactive, conversely in response to high mechanical stimuli, like in cells perceiving a rigid ECM, or a dynamic stretch, YAP/TAZ can enter the nucleus and activate transcriptional activity[69].

While YAP/TAZ are typically activated by mature integrin adhesions, in specialized tissues other mechanosensitive membrane proteins can also relay mechanical signals from the ECM, such as dystrophin-glycoprotein complex (DCG) in the sarcolemma or mechanosensitive ion channels (Piezo) of neural stem cells[67]. YAP/TAZ are further impacted by multiple other signaling pathways, most notably the hippo kinase cascade, the first YAP/TAZ regulation mechanism to be discovered[66] . Hippo signaling inhibits YAP by phosphorylation through the activity of kinases (Large tumor suppressor Lats1/2), and is induced by proteins involved in cell-cell junctions and cell polarity[67].

Overall, YAP/TAZ activity is under tight control of the various inputs provided by the mechanics and structure of the cell environment[70], placing YAP/TAZ as an ideal molecular beacon, integrating how the cell responds to the multiple physical signals originating from its surroundings.

YAP/TAZ nuclear retention has also been reconducted to the capability of mechanosensitive cells to display a “mechanical memory” from lengthy exposure to a stiff environment: when detached and plated onto soft substrates, these cells maintain a response typical of the previous mechanics, influencing cell migration[71], epithelial-mesenchymal plasticity[71] and stem cell differentiation[72].

Alteration of YAP/TAZ activity by tissue mechanics has far reaching effects on several diseases, for instance, sustained YAP/TAZ activity from tissue stiffening has been shown to induce in-vivo conversion of quiescent fibroblasts into TGF-β induced profibrotic myofibroblast in liver[73], lung[74] and renal fibrosis[75].

The nucleus in mechanotransduction

The nucleus is the stiffest and largest organelle in the cell. Nuclear mechanics, morphology and function are greatly impacted by the nuclear lamina, a network of intermediate filament protein fibers (lamins) underlying the inner nuclear membrane, that functions as a structural element. Integrated in

the nuclear envelope, and tied to the nuclear lamina, the linker of the nucleoskeleton and cytoskeleton (LINC) proteins, mechanically couple the nucleus to the three main kinds of cytoskeletal filaments[52].
Together with its central role in gene expression, recent studies have highlighted the key role of the nucleus as a mechanosensitive organelle[76]. In particular a direct role of the nucleus, as a "internal ruler" of the extracellular environment has been advanced[77], in this view, when the nucleus is squeezed, the nuclear envelope stretches, opening nuclear pores that enable the export of calcium and contractility-enhancing signals. Thus cells can tune their mechanoresponse through the plasticity of the nucleus, for instance through different expression levels of lamins[78,79].
The involvement of this mechanism in the regulation of YAP/TAZ nuclear import and of other mechanosensitive transcription factors, was supported by experiments showing that direct force application the nucleus is sufficient to induce YAP activation[80].
The modulation of the mechanical properties of the nucleus through lamins is also critical in preventing envelope rupture resulting from mechanical challenge to nuclear integrity, as in restricted migration through micropores[81].
In addition to the contributions of the nucleoskeleton, perinuclear cytoskeletal structures also play a determinant role in shaping the nucleus: in dendritic cells perinuclear actin dependent on Arp2/3 allows nuclear deformation despite a rigid, lamin A/C rich envelope, permitting migration through micrometer sized channels[82]. In fibroblasts, stress fibers of the actin cap overlay the nucleus and are essential in regulating nuclear shape in response to stiffness[83].
At the termini of the actin cap stress fibers, distinctive focal adhesions have been singled out as mechanosensing elements, characterized by higher turnover, distinct composition[84] and higher cell traction forces[85], suggesting a tension enhancing role of the nucleus in this architecture.

Substrate rigidity sensing

An impactful source of mechanical signals is the rigidity of the ECM: the resistance it opposes to deformation. The ECM mediates the forces originating from the cell surroundings[86], but even in absence of externally applied forces, cells continuously probe this feature of their environment, by engaging the ECM with integrin FAs and exerting traction on them, mainly by means of actin polymerization against the cell membrane and actomyosin molecular motors[6,87]. This induces conformational changes in mechanosensitive proteins such as talin[88], triggering the recruitment of signaling and actin-linking proteins, and adhesion reinforcement through integrin clustering[25].
Although talin has been shown to be an indispensable for the formation of adhesions[39] and appropriate sensing of substrate stiffness[89] and stretching[62], stiffness sensing also depends on intracellular tension

by actomyosin contractility[90] and numerous experimental studies point to lamellipodial[57] and filopodial[91,92] contractile elements at the cell periphery, as mechanosensing units[93], however perinuclear adhesions have also been singled out as key players in substrate sensing through their direct mechanical connection to the nucleus via the actin cap[85].

Responses to stiffness such as changes in morphology or proliferation are dependent on cell type[94] and malignant transformation of cells often involve alterations in the mechanosensory systems of the cell: such as loss of anchorage-dependent survival and enhanced contractility and deformability[10,95]. In fact, substrate mechanosensing can be tuned by multiple factors, both cell extrinsic (ECM type[96], ligand density[97]) and cell intrinsic (contractility[98], cytoskeletal "rheology"[99], expression of different integrin types[26]).

Although the effects of environmental stiffness have been extensively investigated, it is a passive feature of the substrate, and which are the actual physical variables directly perceived by cell is still debated[62,100]. Often, the way cells regulate force transmission with the matrix has been rationalized in the framework of the molecular clutch model: the different rates of binding and unbinding of the molecular bonds engaging the substrate (ECM-integrins) with the contractile units of the cell (integrins-cytoskeleton) as a function of force, determining the threshold of rigidity at which force transduction takes place[101]. If adequate forces are provided, upon engagement of the clutch, talin unfolds and exposes vinculin binding domains[88], and downstream signaling leads to adhesion reinforcement through integrin clustering and actin crosslinking (avoiding the disengagement regime predicted by the model at high rigidities)[89].

The centrality of the dynamic, mutual interaction between the ECM and the cells residing in it in guiding tissue development and responses to wounds and disease has been long recognized[102], in fact the force sensing system of cells is highly dynamic: external forces applied to integrins produce cytoskeletal reorganization in under one second[103], and deformations propagate to the nucleus[104], changes in the composition and size of FA happening under one minute from force application[31,32,105] and inhibition of cell contractility is closely followed by reduced adhesion size[40]. During long term processes, such as cell spreading or proliferation (encompassing several hours), cells continuously probe the environment in cycles at the minute timescale and adjust their traction forces accordingly[106].

The dynamic adaptability of the cell can be understood in the context of the tensegrity model, the cell itself, and its various structural elements, constituting a modular tensegrity system[52]. If adhesive and mechanical stimuli are present, cells assume a stable structure, its shape maintained by a state of tension "prestress", that also permits reversible changes to respond to outside perturbation. Since the entire structure is connected by tension-transmitting elements, a local force produces an integrated

structural response, enabling rapid transmission of signals that outpaces diffusion-limited signaling molecules[52].

Biomaterials in mechanobiology

The complexity of the in-vivo cell environment, makes it necessary to develop systems that allow systematic control over the diverse stimuli that cells experience, in order to elucidate their contribution to cell responses. In this optic, many biomaterial platforms have been devised to reproduce in vitro the salient biophysical features of the ECM, like hydrogels, but also allow to exert forces onto cells (stretching membranes) or measuring traction forces cells apply to their substrates.

Hydrogels

Hydrogels are soft materials composed of a polymer highly hydrophilic network, suspended by a huge amount of water: this broad definition encompasses both systems where the network is given by physical interactions (entanglements, ionic interactions) and chemical gels, where covalent bonds establish crosslinks between polymer strands.

Hydrogel materials serve key roles in many seminal mechanobiology studies: examples include the fabrication of ECM coated substrates to gauge the effect of different stiffnesses on cell migration and differentiation[3,4] and measurements of forces exerted by cells on the substrate by traction force microscopy, by recording the displacements of reference beads embedded in the gel[107].

From a mechanobiology standpoint, the main advantages of hydrogel materials reside in their similarity to the in-vivo ECM of soft tissues and the tunability of their mechanical properties.

As for the former aspect, decellularized ECM or purified ECM constituents have been used to prepare hydrogels better resembling the physiological environment. However, they offer a narrow range of mechanical properties, depending on multiple variables such as source tissue, dilution, pH and temperature[108,109]. Also, independent control of mechanical properties and other key features such as the density of cell adhesion ligands is difficult for integrin-binding proteins such as collagen[110].

As a result, hydrogels having defined mechanical properties are usually prepared by polymerization and crosslinking reactions of chemically modified natural polymers or from synthetic precursors (monomers or macromers).

The requirement of cytocompatibility restricts the available synthetic strategies to produce hydrogels, especially if the materials are developed for cell embedding. This has restricted the choice of material and crosslinking chemistries for the synthesis of substrates for mechanobiology research.

Synthetic polymer hydrogels

Synthetic, hydrophilic polymers are invaluable building blocks for hydrogel scaffolds for multiple reasons: their structure and properties are easier to control with respect to naturally derived substances and they are often biologically inert. As such they constitute "blank slate materials", that can be engineered with bioactive moieties, such as peptides promoting cell adhesion, enzyme-degradable crosslinks, and growth factors[110] allowing fine and independent control of the various cues the hydrogel provides to cells.

Polyacrylamide (PAA)

Polyacrylamide (PAA) hydrogels have been among the first synthetic soft substrates (along with silicone films[111]) that have found applications in mechanobiology studies.
PAA hydrogels are typically obtained by radical chain polymerization of the monomer acrylamide (AA), with crosslinking molecules, the most common being bis-acrylamide (BA) (Scheme 1), although other molecules with multiple double bonds have also been used[112,113].

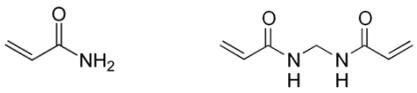

Scheme 1: structures of the acrylamide (left) and bis-acrylamide (right) monomers

As the initiator system, ammonium persulfate (APS) is usually employed in conjunction with tetramethylethylenediamine, (TEMED) the latter acting as a catalyst for the generation of radical species (Scheme 2).

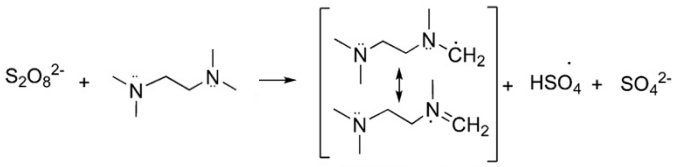

Scheme 2: TEMED-promoted generation of radicals from persulfate

Since the AA monomer itself and the radicals produced during polymerization are hazardous to cells, PAA hydrogels are first polymerized and then extensively washed before using them in cell cultures. This precludes cell embedding, and 3D environments can only be approximated by surrounding cells between two layers of pre-cast gels (sandwiching)[114].

The mechanical properties of the gel are usually adjusted by variation of the total amount of monomers and the ratio of AA to BA. In the scientific literature obtainable values of stiffness and porosity are collected, with E values ranging from as low as a few Pascals up to hundreds of kPa[115-117]. The stiffness of the gels typically raises with the concentration of total monomers and percentage crosslinker content, however excessively high BA concentrations can lead to structural inhomogeneities that decrease the overall elasticity of the network[116] and result in turbidity[112].

As PAA surfaces repel proteins, and block nonspecific cell adhesion, various coupling strategies have been applied for introducing cell-adhesive ECM proteins or peptide sequences to PAA. One of the most common procedures involves the usage of sulfo-SANPAH, a heterobifunctional crosslinker containing a UV-photoreactive group, allowing binding to polyacrylamide, and a N-sulfosuccinimidyl ester group that undergoes conjugation with amine groups of proteins[117].

Improvements on this protocol have been proposed, such as the incorporation of primary amine groups in the hydrogel network to enhance the coupling efficiency[118], and alternative methods enabling protein conjugation without UV activation, for example using 2-pyridinecarboxaldehyde functionalized monomers[119].

The phenomenon of durotaxis, cell migration directed by differences in surface stiffness, was demonstrated using PAA substrates with a stiffness gap, introduced by polymerization of two adjacent precursor solutions with differing crosslinker content[4], or with a gradient stiffness, obtained by photopolymerization using a photomask with an opacity gradient[120-122].

PAA hydrogels were also used to develop a wound model with controllable stiffness, that does not require scratching the culture substrate, by placing a removable PDMS barrier on top of the gel[123].

Poly ethylene glycol (PEG)

Poly ethylene glycol (PEG), also termed poly-ethylene oxide (PEO), is a flexible, hydrophilic polymer obtained from ethylene oxide. The main advantages of using PEG as a building block for hydrogels, reside in the availability of a broad spectrum of macromers having good biocompatibility, defined molecular weight and structure (linear, multi-arm) and the ease by which the terminal hydroxyls can be converted into different functional groups, allowing diverse bio-orthogonal chemistries for crosslinking or biomolecule derivatization. PEG hydrogels have been applied for 2D cell culture and

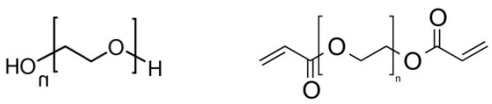

Scheme 3:structure of linear PEG polymer (left) and PEGDA crosslinker (right)

inclusion of cells in 3D scaffolds (using PEG monomers as the sole component or in conjunction with other polymers, with PEG constituting the crosslinker or a spacer moiety for ligand presentation).

This wide landscape of PEG functionalities is reflected in the multiple approaches that have been exploited to obtain PEG-based hydrogels. Common synthesis procedures include: free radical polymerization, usually using acrylate macromers such as PEG diacrylate (PEGDA), in conjunction with photoinitiators[124], radical promoted thiol-ene reactions[125] and Michael-type additions such as thiol-ene reactions[126,127].

When photoinitiators are employed to prepare hydrogels, several factors can result in cell damage: together with the toxicity of the initiator and its by-products, the effects of radiation need to be considered. Initiators such as LAP and Irgacure 2959 have been broadly used, as they require moderate light exposure[124] and due to their cytocompatibility[128].

PEG based gels have been used to show that functionalization with RGD peptides directly coupled to the polymer backbone results in poor, non-specific cell adhesion supported by adsorbed protein, whereas introducing a spacer enhanced cell spreading through RGD specific cell adhesion[129].

Naturally derived hydrogels

Hyaluronic acid

Hyaluronic acid is a non-sulfated GAG, found ubiquitously in tissues, and particularly enriched in the ECM of soft tissues (synovial fluid in ligaments, vitreous body), its functions being mainly water-retention, viscosity enhancement and lubrication[130].

In the ECM, it is usually present as linear, high molecular weight polymer (10^5-10^7 Da)[131]. At physiological pH, the acid groups are hydrolyzed, resulting in a highly hydrated polyanion.

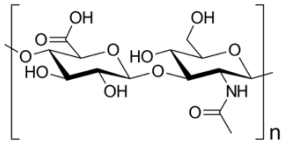

Scheme 4: structure of hyaluronic acid

As native HA does not exhibit significant elastic behavior, strategies for introducing crosslinks to stabilize HA into hydrogels.

The functional groups that are present in the native HA structure represent useful chemical handles that allow a broad range of modifications , that can be exploited for the fabrication of scaffold having diverse structures and mechanical properties[132]: the hydroxyl groups can be directly esterified, introducing methacrylate groups[133,134], affording photocrosslinkable polymers, and the carboxylic acid

can react with amines[135] or hydrazides[136] by carbodiimide mediated reactions, allowing crosslinking or coupling with bioactive molecules.

Thiolated HA are of particular interest, as disulfide bonds can be introduced by mild conditions, such as oxidation by air exposure, affording gels that can be applied for cell encapsulation[137]. While this approach involves long reaction times or aggressive oxidant agents, the same thiolated HA can also react in a Michael-type addition to crosslinkers containing double bonds, such as PEGDA, allowing rapid crosslinking [138] and functionalization with RGD to enable integrin adhesions[139].

HA hydrogels have been applied in several mechanobiology studies: HA was crosslinked and coupled to fibronectin domains using PEGDA, to prepare hydrogels having defined mechanical properties (G' = 0.2 – 4 kPa). These substrates were used to study the effect of stiffness on fibroblasts cellular mechanics (stiffness and traction forces) and proliferation[140] . Michael type addition can be also used to directly functionalize methacrylated HA with cysteine containing peptides, an example being a HA platform that was used to dissect the contributions to MSC mechanosensing by cell-cell interactions, presenting a small peptide sequence from N-cadherin, and cell-ECM adhesions (RGD)[141].

Michael addition chemistry was also used to obtain a brain-mimetic 3D matrix, that was synthetized by crosslinking RGD-functionalized methacrylated HA with DTT. Matrices having different stiffnesses (50 Pa to 35 kPa) were used to incapsulate glioblastoma spheroids, that exhibited rigidity-dependent migration and proliferation[142].

Although HA does not directly support integrin-mediated adhesion, it is still a bioactive polymer: it is recognized and internalized by cells through specific receptors such as CD44[143], and it is the substrate of hyaluronidase enzymes, involved in ECM remodeling[144,145].

For instance, FN coated HA hydrogels have been shown to enhance mechanotransduction in multiple non-transformed cell lines compared to PAA hydrogels[146] and HA matrices enhance MSCs chondrogenesis compared to an inert polyethylene glycol (PEG) scaffolds with similar mechanical properties[147]. It was found that HA interactions prelude and modulate integrin-based adhesions in chondrocytes[148] and glioblastoma cells[149,150].

Mechanical properties of hydrogels and their characterization

The interactions making up the network result in markedly different mechanical properties of the gel, and different responses to stimuli: for instance, physical gels can fully dissipate mechanical stresses (given enough time) and can dissolve under mild conditions (such as changes in temperature, or ionic strength), while covalent hydrogels are more rigid and are typically irreversible.

The mechanics of hydrogels are impacted by their multi-phase nature: although they contain a significant amount of water, it is sufficiently retained by the network so it does not readily flow like a liquid, and their mechanical properties are significantly poorer than common solid materials. In fact, they exhibit nonlinear stress (σ)-strain (ε) behaviors and time-dependent responses (viscoelasticity).
In the field of mechanobiology, stiffness has been typically identified with the elastic behavior of the material[5], in particular the Young's modulus E, that can obtained from uniaxial compressive or tensile testing as the slope of the stress-strain curve in the linear region of deformation (for small strains):

$$E = \frac{\Delta\sigma}{\Delta\varepsilon}$$

for instance, in one of the early implementations of PAA hydrogels for cell culture Wang[3] obtained the elastic moduli of a range of composition by traction measurements of gel cast as sheets and deformed applying a known weight with a clamp. Measurements of elasticity can also be obtained from shear tests like rheometry as the shear modulus G, which is related to E through Poisson's ratio v.

$$E=2G(1+v)$$

Gels can be approximated as homogeneous materials with v = 0.5 for sufficiently rapid deformations, lower Poisson ratios result in the case of slow deformation rates due to water flow through the network[151]
There are number of practical obstacles in handling hydrogel samples for collecting tensile measurements, as hydrogels tend to break or slip, and can deform under their own weight. Also, their mechanical properties are highly dependent on their degree of swelling, so their moisture needs to be controlled during such measurements.
The mechanosensitive elements of the cell, such as nascent adhesions or contractile units, can have dimensions as small as 100 nm, accordingly, cells can sense the underlying material properties features of comparable size[152], and stiffnesses at a depth that has been estimated to range from a few micrometers[153] to dimensions comparable to the cell area[154]. As a result, (sub)micro-scale techniques have been applied to characterize the surface of biomaterials, with the possibility of collecting maps of mechanical properties at nano-scale resolutions, such as AFM[155] and nanoindentation[156] methods.
While gel behavior can be approximated as linearly elastic, this holds only in the linear viscoelastic regime, valid only low deformations and frequencies, and recent studies have highlighted the impact of viscoelastic (time/frequency dependent) properties on cell behavior[157,158].

Dynamic hydrogels

According to the tensegrity model, the architecture of the cell continuously adapts to changes of their environment by reversible perturbations[52]. Instead, in classical stiffness assays, cells are plated on static hydrogels, by first detaching them from a typically super-physiologically stiff culture substrate, or dissociating them from tissue, greatly disrupting their cytoskeletal architecture. Enzymatic dissociation can also lead to loss of (integrin) receptors on the cell surface and lower the strength of adhesions to the substrate[159]. Additionally, diverse cell types display a "mechanical memory" effect, that biases their response after extended periods of culture on stiff substrates[72,160].
Thus, to better mimic a gradual adjustment of cells to the dynamic evolution of ECM mechanics, culture substrates allowing controllable changes of their mechanical properties in the presence of adherent cells are preferrable.

Light-controlled dynamic hydrogels

For this class of materials, strategies to realize in-situ dynamic hydrogels are mainly based on photoreactions that increase or decrease the crosslinking degree.
For material softening, photocleavable moieties such as o-nytrobenzyl esthers (Scheme 5) have been exploited to obtain on-demand softening of PEG-based[161] and PAA-based[162,163] hydrogels.

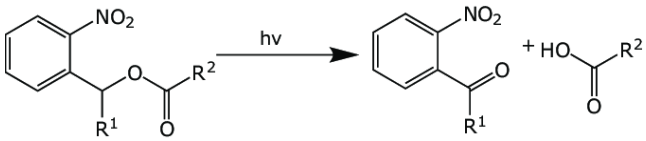

Scheme 5: photoinduced cleavage of the o-nytrobenzyl esther bond

The advantage of this approach resides in the high spatial resolution of the degradation process, as o-nytrobenzyl esters (o-NB) can undergo two-photon photolysis[164], on the other hand, the portion of the gel that can be modified is limited by the irradiation area, and for 3D applications the absorption of light throughout the material limits the attainable depth of softening.
A PEG-based hydrogel obtained with an acrylic ester of o-NB, allowing in situ softening form 10kPa to 2kPa was instrumental in advancing the concept that MSC differentiation is influenced by a "mechanical memory" effect: in fact a high enough mechanical dose (days in culture on the stiffer gel) leads to persistent YAP activity, biasing differentiation towards an osteogenic fate even when the substrate is ultimately converted to a mechanically deactivating (soft) state.[72]

A similar photodegradable PEG hydrogel system allowing in situ softening from 32kPa to 7kPa was used to show how substrate softening can induce valvular interstitial cells to revert from a myofibroblast phenotype (associated with cardiovascular disease) to a quiescent fibroblast one.[165]

Alternatively, photoinitiator-promoted reactions can be exploited to remove crosslinks: for example allyl sulfide crosslinks can be cleaved by radical addition-fragmentation chain transfer[166], initiated by

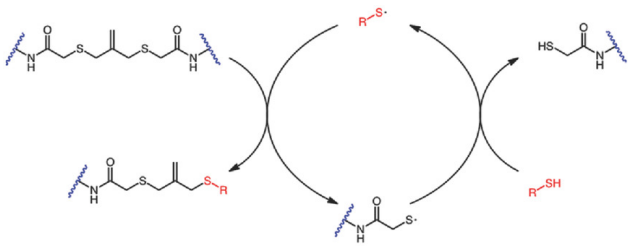

Scheme 6: radical promoted cleavage of allyl sulfides

UV light irradiation of LAP in the presence of soluble thiols.

While this approach requires two additional soluble species to the system, the main advantage, compared to direct photolysis, resides in improving the efficiency of the process: given by the chain propagation nature of the reaction, low photoinitiator concentration are required, thus limiting light absorption, and the extent of degradation can be tuned by changes of the thiol concentration[167].

This strategy was exploited to obtain PEG based hydrogels allowing rapid softening of the elastic modulus from 32.7kPa to 5.5kPa. This substrate was used to show that stiffness-induced epigenetic chromatin modifications in hMSC can be reversible depending on mechanical dosing (culture time, in days, on the stiffer condition).

For photo-stiffening materials, additional crosslinks can be introduced through residual reactive groups from the gelation reaction. For instance, in a HA based hydrogel, methacrylate groups were partially crosslinked by a Michael-type addition with a limiting amount of DTT crosslinker, allowing subsequent photopolymerization raising E from 3kPa to 30kPa. hMSC cultured on the soft substrate and stiffened at later days showed increased differentiation bias to adipogenic differentiation the longer they experienced a soft substrate[168]. A similar material ranging from 0.1 to 3 kPa was used to study the stiffening-induced EMT behavior of epithelial spheroids (MCF10A)[71].

Using a similar strategy, photostiffening hydrogels were prepared through a SPAAC reaction between 8-arm DBCO terminated PEG and azide-functionalized 4arm-PEG, the residual alkyne groups from gelation allowed LAP-mediated photostiffening ranging from 2-16 kPa to 32 kPa.

This hydrogel system was used in conjunction with primary muscle stem cells to recapitulate the effect of muscular tissue stiffening following injury[169].

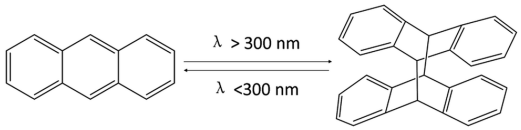

Scheme 7: anthracene dimerization

Alternatively, the introduction of additional crosslinks can entail photoreactions of different chemical groups (one example being anthracene dimerization (Scheme 7) which was introduced in a PEG hydrogel to achieve photostiffening from 10 to 50kPa and study the effect on the NFAT transcription factor, involved in mechanosensitive calcium signaling[170].

Another approach involves the polymerization of a secondary network, as with PEG-based hydrogel that was prepared by first embedding cells in a soft matrix crosslinked with metalloproteinase-sensitive peptides and subsequently photopolymerizing a secondary network using thiol and norbornene-functionalized 8-arm PEG monomers network[171].

Light controlled tuning of crosslinking degree can also be used to obtain materials that allow reversible stiffness control, for instance, a hydrogel was prepared from a doubly functionalized HA, allowing a stiff-soft-stiff (14.8-3.5-27.7 kPa) sequence[172]. In this system the difference in reactivities of acrylate and methacrylate in Michael-type additions has been exploited: o-NB moieties connected to the more reactive methacrylates were first crosslinked by reaction of DTT to obtain a gel and, after photosoftening, the crosslinking degree was enhanced by a LAP mediated reaction of acrylates.

A different approach for stiffness phototuning involves molecules that undergo conformational

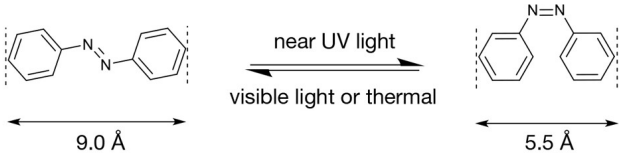

Scheme 8: light-promoted azobenzene isomerization

transitions when exposed to light, one example being azobenzene, a compound that converts from the E isomer to the Z one upon exposure to UV radiation, and returns to the original structure with thermal relaxation or exposure to visible light (Scheme 8).

The azobenzene moiety has been exploited to achieve PEG-based173 and PAA-based174 hydrogels that can withstand multiple cycles of softening-stiffening, however the overall change in modulus was modest for the PEG system (in the order of 200 Pa, G') and for the PAA system, only the stiffening effect was investigated, as the UV dose required for softening was found to be incompatible with the hMSC used in the study. Indeed, a major drawback of many light controlled system is that most photosensitive reactions require UV or blue light, with potential of phototoxicity. In fact studies

employing light-controlled systems are often validated by monitoring the effects of light exposure on the cells of interest, such as assays for viability or DNA damage[168,173,174].

Recently, materials that respond to lower energy light have been explored: an example being a PEG based hydrogel, where light-responsive crosslinks were introduced by coupling protein domains from cyanobacterial photoreceptor Cph1, that undergoes a conformational change under red light (660nm) favoring dimerization and increasing stiffness. Upon irradiation with far red light (740nm) the transition is reversed and the hydrogel softens from 18 kPa to 14kPa[175].

Hydrolysis/Enzymatic activity for dynamic hydrogels

Synthetic PEG hydrogels can be subject to network degradation by non-specific hydrolysis (for instance of the ester groups from acrylate monomers such as PEGDA), however the process is relatively slow under physiological conditions[176], and the otherwise uncomplicated temporal control of the process through pH or temperature is potentially harmful for cells. Instead, control of the network degradation time can be achieved by changes in the network structure, such as co-polymerization to obtain blocks of more reactive PGA and PLGA chains[177], or changing the chemical environment of the hydrolysable groups[178]. This strategy has been employed to overcome the constraints imposed on cell growth in three dimensional PEG matrices[178,179].

Hydrolytic softening gels based on hyaluronic acid have been applied to study the stiffness dependent behavior of hepatic stellate cells, in a model of liver fibrosis regression, however the process involved 14 days of degradation without the possibility to tune the timing of the process[180].

Another strategy that enables hydrogel softening , especially relevant for 3D cell culture, is the introduction of enzyme-cleavable peptide crosslinkers, that allow cells to grow and migrate through the matrix[181]. While the effect of this cell-controlled modulation of matrix properties, has far reaching consequence in matrix-confined cell and organoid cultures[182,183], it does not readily allow external control over the softening process.

(Bio)molecule-controlled dynamic hydrogels

In situ modulation of substrate stiffness can also be achieved through soluble small molecules.

The glycation of proteins (crosslinking of proteins with reducing sugars), has been used for stiffening of Collagen I matrices in a model for tumor-induced ECM crosslinking[184], however the process requires several days if the concentration of sugar is kept at cell-tolerable levels[185].

Divalent cations such as calcium can form crosslinks between guluronate groups in alginate chains, for instance, formation of an interpenetrating polymer network (IPN) within a basement membrane

extract (matrigel) was applied to achieve stiffening of a 3D scaffold independently from ligand density in a model of stiffness induced malignancy of mammary epithelium[186].

This strategy can also be modified to achieve spatial control of the process, for instance the photothermal effect of gold nanorods has been exploited to obtain NIR irradiation-triggered release of chelators from liposomes, and soften an alginate hydrogel[187].

RESULTS

Several obstacles prevent the widespread usage of hydrogel supports for biological assays, despite the advantages offered by this class of biomaterials. Conventional hydrogel preparation and characterization protocols, with defined static rigidities or in situ modulable mechanical properties, are fairly complex, requiring synthetic and advanced material science expertise and/or dedicated equipment (AFM, UV light sources), thus limiting the ease of access to these protocols to the biological community.

Furthermore, while there is considerable evidence on the effects of cell behavior modification due to substrate elasticity, recent publications in the field contained seemingly contradicting conclusions on which other biophysical features of cell culture substrates (ligand density, substrate porosity, protein tethering)[188,189] predominantly impact on cellular mechanosensing.

The aim of the present work is the development and application of hydrogels platforms having static and dynamic stiffnesses, establishing easily implementable and reliable fabrication procedures and using them for cell mechanobiology studies.

PAA-OH (Hydroxyl-functionalized polyacrylamide hydrogels)

Synthetic hydrogels having defined stiffness and coated with ECM proteins (such as fibronectin or collagen) for cell attachment are instrumental in mechanobiology studies. However established protocols for the fabrication of these substrates pose a number of complications we here sought to overcome: covalent coupling strategies rely on coupling reagents such as sulfo-SANPAH, that require dedicated equipment for UV activation and are unstable, or functionalization of monomers with N-succinimidyl ester prior to polymerization[190], overall these steps negatively impact the scalability of the process.

Conversely, hydroxyl-functionalized polyacrylamide hydrogels (PAA-OH), are readily prepared by introducing an inexpensive reagent, N-Hydroxyethyl acrylamide (HEA) in the prepolymer solution, and allow hydrogen bond interactions for the attachment of proteins, in fact cell-adhesive proteins have been patterned on PAA-OH hydrogel substrates through micro-contact printing methods[191].

By introducing HEA and varying the concentration of acrylamide and bis-acrylamide, we obtained hydrogels with a broad range of elastic moduli, and similar mechanical properties to conventional PAA substrates (Table 1).

To further characterize the materials structure, the diffusion of fluorescent probes of defined size (

Table 2) into the swollen hydrogels was used to characterize the range of mesh sizes for each of the compositions (Figure 4).

Table 1: PAA-OH hydrogel formulations, with corresponding elastic modulus measurements collected with the micropipette aspiration method and meash size as determined by permeation or exclusion of fluorescent probes.

Hydrogel	AA wt%	BA wt%	E PAA-OH [kPa]	Mesh size [nm]
PAA-OH1	3.5	0.03	0.32 ± 0.03	61.83-100
PAA-OH2	3	0.15	3.15 ± 0.27	22.63-31.64
PAA-OH3	5	0.15	6.09 ± 1.35	9.33-12.23
PAA-OH4	5	0.225	13.39 ± 1.73	9.33-12.23
PAA-OH5	8	0.48	50.01 ± 3.07	<9.33

Table 2: molecular weights (Mw), intrinsic viscosity and corresponding hydrodynamic radii (Rh) of the FITC-dextran probes used for mesh size measurements (See Methods section for the derivation of the parameters).

Mw [g/mol]	η [mL/g]	Rh [nm]	d [nm]
40000	1.60	4.67	9.33
70000	2.06	6.12	12.23
250000	3.66	11.32	22.63
500000	4.99	15.82	31.64
2000000	9.32	30.92	61.83

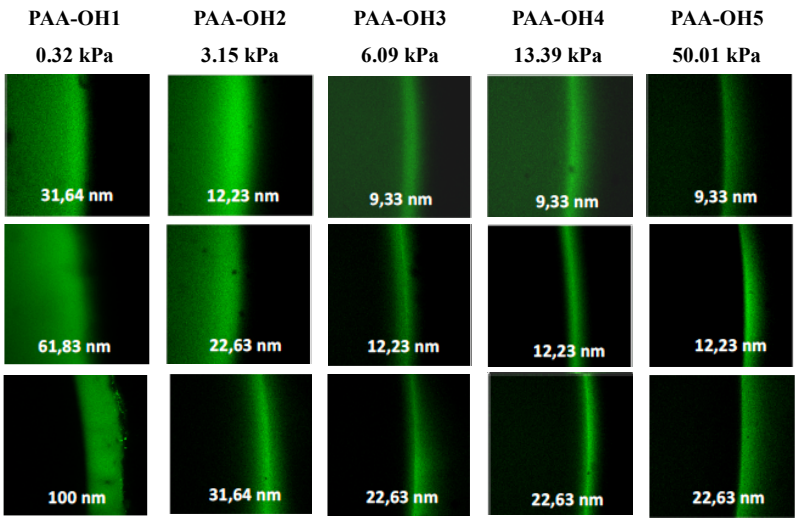

Figure 4: Representative confocal images of the PAA-OH gel (left)-solution(right) interface used to evaluate the cut-off values of mesh size for the reported compositions, the diameter of the probe is reported at the bottom of each picture

For the coating strategy, as contact printing requires specialized equipment, we opted to introduce the ECM protein through a direct adsorption coating method, by incubating the hydrogels in a fibronectin solution. We can conclude that the improved efficiency of protein coating was due to the introduction

of the functional co-monomer HEA by performing the same procedure on PAA hydrogels without hydroxyl groups as controls (Figure 5).

The coating procedure was also successfully applied with a different ECM adhesion protein, laminin, confirming the versatility of the procedure (Figure 5).

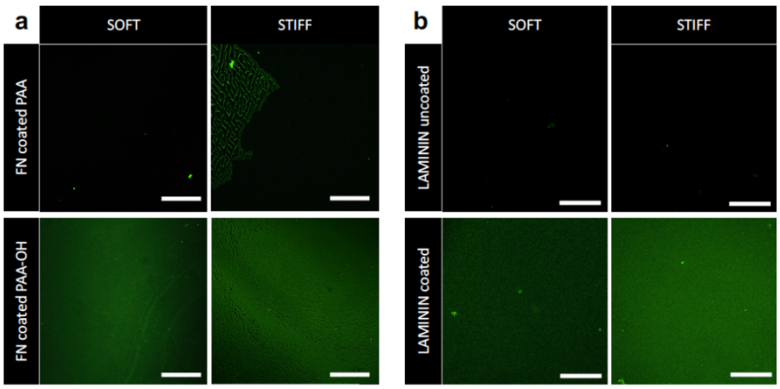

Figure 5: a) visualization of fibronectin coating on PAA-OH hydrogels by AF488-coupled fibrinogen b) visualization of laminin coating by IF staining, soft condition corresponds to PAA-OH1 and stiff conditions to PAA-OH5

To obtain homogeneous fibronectin coating, it was essential to control the substrate drying conditions before cell seeding. This was particularly evident by observing YAP/TAZ localization on soft hydrogels, as with an excessive drying time (>15') cells exhibited nuclear localization despite the underlying substrate had stiffness values definitely insufficient to support mechanical activation of YAP/TAZ. Visualizing the coating distribution on gels vs drying times, by incubation with AF488 labelled fibrinogen, showed that fibronectin assembled in fibers, exposing an uneven distribution of adhesive cues and overshadowing the intended low mechanics of soft substrates (Figure 6).

Having established a suitable coating procedure, we then used YAP/TAZ localization as an immediate and quantitative proxy of cell interactions with these hydrogels, monitoring the effect of a range of stiffnesses on two different cell lines: immortalized mammary epithelial cells MCF10A and transformed osteosarcoma U2OS cells. YAP/TAZ activity was quantified by immunofluorescence imaging, through the ratio of nuclear over cytoplasmic signal. (Figure 7). We found that for both cell types, YAP/TAZ localization closely followed the trend in stiffness of the set of hydrogels, hereby validating the fabrication protocol. The set of materials afforded a full range of YAP/TAZ responses, from predominantly cytoplasmic for the softest (0.32 kPa) hydrogel to mainly nuclear for the stiffest one (50.01 kPa).

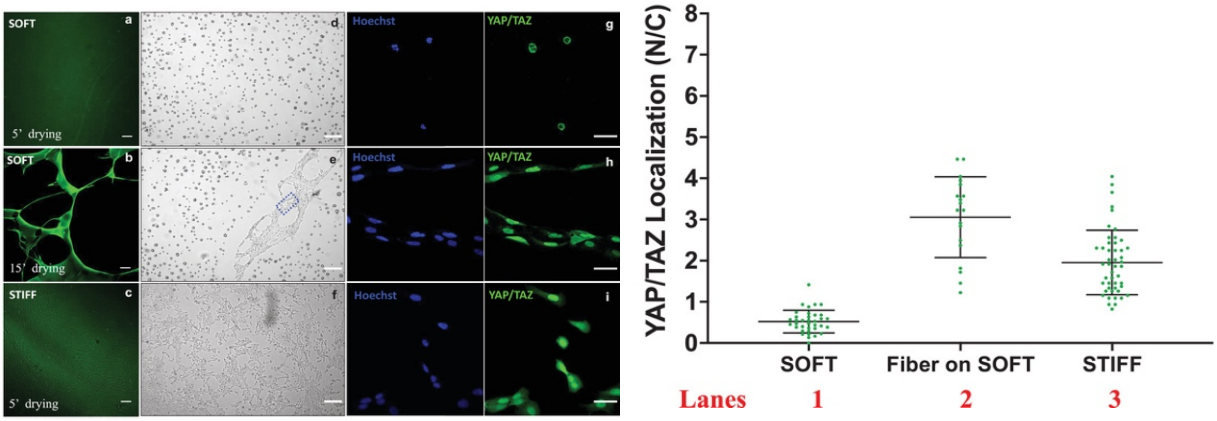

Figure 6: Fluorescence images of the PAA-OH substrates coated with a solution of fibronectin (FN, 25 μg mL−1) and Alexa488 conjugated Fibrinogen (2 μg mL−1), for two different stiffnesses (a,b: soft 0.32 kPa, c: stiff, 50 kPa) and two drying times (for the soft hydrogel) after FN incubation. For each picture it is shown an example of cell (MCF10A) seeded on that substrate (bright field images d–f). FN fibers are visible in the rectangle of figure e. YAP/TAZ staining of U2OS cells seeded on: soft PAA-OH (g), FN fibers conjugated to soft PAA-OH (h) and stiff PAA-OH (i). From the staining are visible: nuclei (in blue) and YAP/TAZ (in green). l) quantifications of the Nuclear to Cytoplasmic ratio (N/C) of YAP/TAZ subcellular localization in U2OS seeded on soft PAA-OH (0.32 kPa), FN fibers conjugated to soft PAA-OH (0.32 kPa) and stiff PAA-OH (50 kPa). Number of cells for each lane in Figure 2l is: lane 1:36; lane 2:19; lane 3:48. Scale bar: 100 μm (a–c), 200 μm (d–f) and 50 μm (g–i)

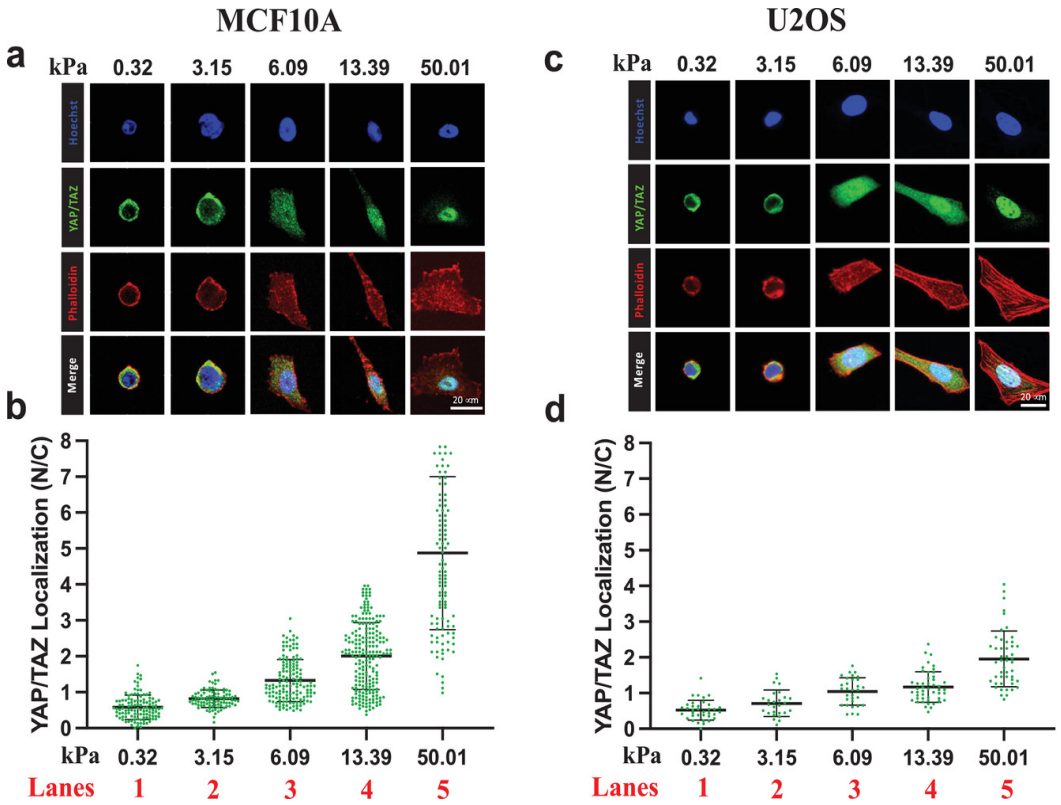

Figure 7: Representative immunofluorescence (IF) images (a,c) and quantifications (b,d) of the Nuclear to Cytoplasmic (N/C) ratio of YAP/TAZ sub- cellular localization in MCF10A (a,b) or U2OS (c,d) cells, after seeding on PAA-OH substrates, coated with FN of five different stiffness. From the staining are visible: nuclei (in blue), F-actin (in red), and YAP/TAZ (in green). F-actin was stained with fluorescently labeled phalloidin to serve as cell shape reference. Each dot in b,d) corresponds to quantification of the N/C ratios of YAP/TAZ subcellular localization in individual cells, as obtained with software-assisted imaging processing of confocal images (see Methods Section). Number of cells for each lanes are: b) lane 1: 116; lane 2: 93; lane 3: 146; lane 4: 210; lane 5: 120. d) lane 1: 36; lane 2: 27; lane 3: 31; lane 4: 48; lane 5: 48.7

PEG-RGD (RGD-functionalized polyethyleneglycol hydrogels)

We then investigated if also a fully synthetic PEG-based hydrogel could allow to be synthesized with a precise and independent tuning of gel stiffness and ligand presentation.

To this end, we used a norbornene (NB) terminated 8-arm PEG as a precursor macromer, crosslinked by di-cysteine peptides and functionalized with mono-cysteine RGD peptides by means of a thiol-ene click reaction, photoinitiated with LAP by exposure to near-UV light. The advantage of these gels is that their chemistry could in principle be used in 3D, embedding cells during the thiolene cytocompatible crosslinking chemistry.

A drawback of related previously reported synthesis, is that the competition of crosslinking and cell adhesive peptides for the same NB moieties, limited the range of stiffnesses below 1 kPa[192]. However, by adapting the concentration of the gel precursors we achieved high elastic moduli even with a relatively high content of RGD peptides (Table 3).

*Table 3: compositions and elastic moduli of the PEG hydrogels [1] Cys/NB molar ratio of the Cysteine (Cys) terminal groups of the cross-linking peptide to the norbornene groups of the PEG macromers. RGD concentration is fixed to 3·10−3M [2] NB-8ArmPEG wt% is the percentage by weight of macromer used to synthesize PEG-RGD hydrogels 3 Stiffness measurements by micropipette aspiration. *Stiffness of PEG-RGD formulations prepared with the synthesis reported in literature (pre-polymerization coupling of RGD peptides to PEG)*

Hydrogel	Cys/NB[1]	PEG wt%[2]	E [kPa][3]	E* [kPa] [3]
PEG-RGD1	0.4/1	4.7	0.30 ± 0.13	0.02 ± 0.08
PEG-RGD2	0.5/1	5.0	0.87 ± 0.13	0.11 ± 0.01
PEG-RGD3	0.6/1	5.2	1.17 ± 0.31	0.20 ± 0.03
PEG-RGD4	0.7/1	5.5	2.63 ± 0.38	0.71 ± 0.08
PEG-RGD5	0.8/1	9.0	7.71 ± 0.38	1.62 ± 0.03
PEG-RGD6	0.8/1	12.5	13.7 ± 0.48	4.47 ± 0.65

To effectively decuple the density of integrin ligands of the substrates from network structure (and its mechanical properties) a cysteine-terminated scrambled peptide, which is not recognized by integrins (containing the RDG sequence), was used to partially substitute the RGD one, while keeping the total peptide concentration constant.

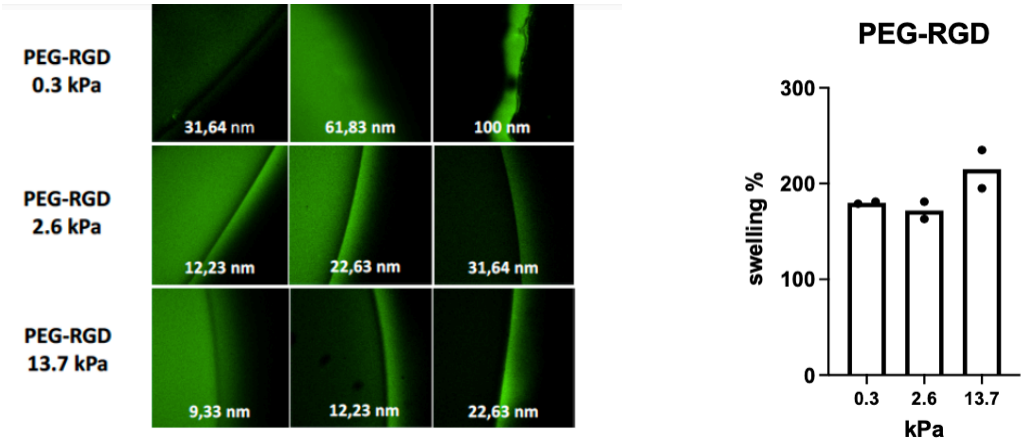

Figure 8: a) Representative confocal images of the gel-solution interface used to evaluate the cut-off values of mesh size for the reported compositions b) hydrogel volumetric swelling measured using an automatic surface approaching sequence of a Netzsch lab+ rheometer with plate-plate configuration for PEG-RGD hydrogels. Samples' thicknesses were measured post- synthesis and after 24h swelling in 1XPBS. For each composition the percentage swelling with respect to the initial height is reported as the mean of two samples.

Finally, we selected a set of hydrogels having low (0.3kPa), medium (2.6kPa) and high (13.7kPa) elastic modulus, to achieve a range of mechanical stimuli representative of the stiffnesses found in soft tissue (respectively low, medium and high) and for each stiffness, three RGD concentrations (1-2-3 mM). To fully characterize these materials, we monitored the impact of the different compositions on the network structure after 24h equilibration with PBS: the swelling behavior and the mesh size were assessed using a set of fluorescent probes having defined hydrodynamic radii
Table 2). The swelling degree was largely constant across the different compositions (Figure 8) and the lateral swelling is minimal[192], due to the thin gels casting attached to glass coverslip. It follows that the RGD ligand superficial density is controlled by the concentration in the precursor solution.

Table 4: range of PAA-RGD hydrogel mesh size, as assessed by exclusion of fluorescent probes evaluated by confocal microscopy

Hydrogel	E [kPa]	Mesh size [nm]
PEG-RGD1	0.3	60-100
PEG-RGD4	2.6	23-32
PEG-RGD6	13.7	<9

The YAP/TAZ activity of U2OS cells seeded on this set of hydrogels was comparable to the ones on PAA-OH substrates, and greatly enhanced with respect to PAA-RGD gels with similar stiffnesses (compare Figure 7 with Figure 10. Using the substrates and U2OS as a paradigm, we gathered several insights: we found that, while the elastic modulus is the overarching mechanical signal controlling

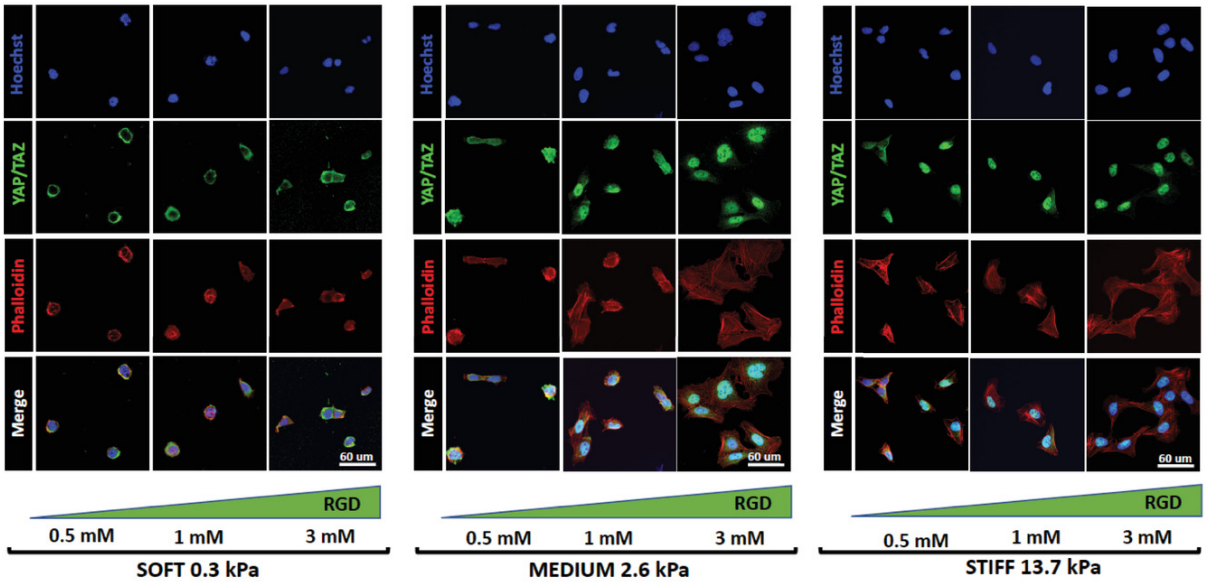

Figure 9: Immunofluorescence (IF) of U2OS plated on PEG-RGD hydrogels at three different values of stiffness and RGD concentration. From the staining are visible: nuclei (in blue), F-actin (in red), and YAP/TAZ (in green). F-actin was stained with fluorescently labeled phalloidin to serve as cell shape reference.

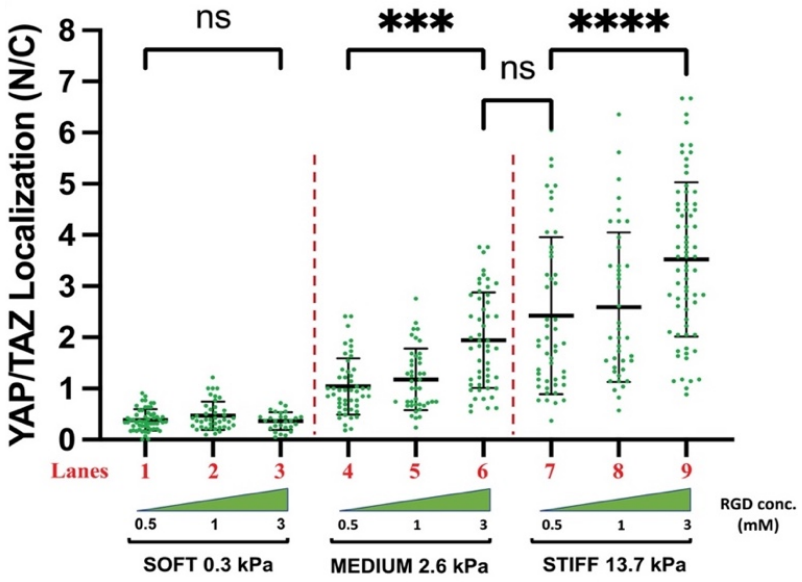

Figure 10: Quantifications of the Nuclear to Cytoplasmic (N/C) ratio of YAP/TAZ subcellular localization in U2OS plated on PEG-RGD hydrogels at three different values of stiffness and RGD concentration. Statistically significative differences were evaluated comparing two groups performing a one-way ANOVA with Tukey's multiple comparison test using GraphPad Prism 9 and considering a confidence interval of 95% (p-values obtained comparing: lanes 1 versus 3, $p = 0.99$; lane 4 versus 6, $p < 0.001$; lane 6 versus 7, $p = 0.3$; lane 7 versus 9, $p < 0.0001$)

YAP/TAZ activity (compare lanes 3,6,9 with 2,5,8 or 1,4 and 7 of Figure 10), increasing the density of RGD sites can enhance mechanosensing (lanes 4 and 6, 7 and 9 in Figure 10) and even compensate for a lower ECM modulus (lanes 6 and 7 in Figure 10). Nevertheless, a minimal stiffness threshold is required to induce YAP/TAZ nuclear localization (as can be seen with low stiffnesses lanes 1-3 in Figure 10).In these experiments immunofluorescence analyses are made after the 24h of culture, and it was found that the changes in YAP/TAZ activity coincide with differences in cell spreading, as assessed by F-actin staining (see Figure 10). However, cells displayed nuclear YAP/TAZ localization even shortly after attachment to the biomaterial surface, while still maintaining a round morphology

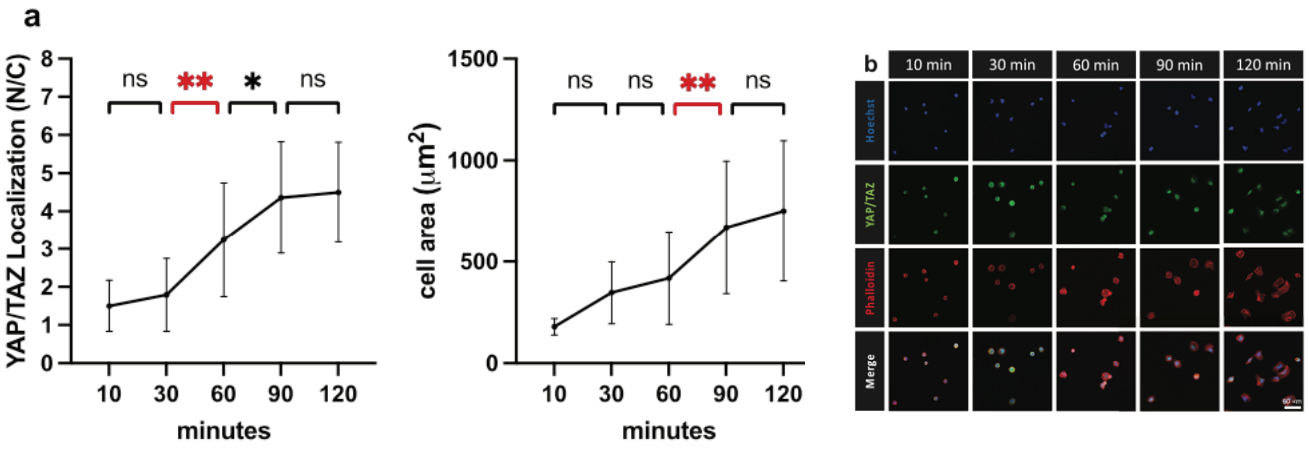

Figure 11: a) Quantifications of Nuclear to Cytoplasmic ratio of YAP/TAZ (N/C) of U2OS cells, as a function of the elapsed time after seeding, on stiff PEG-RGD (13.7 kPa) after 10, 30, 60, 90, and 120 min. Statistically significative differences were evaluated by one-way ANOVA with Tukey multiple comparison. p-values for YAP/TAZ localization: 10 versus 30 min, p = 0.95; 30 versus 60 min, p = 0.003; 60 versus 90, p = 0.047; 90 versus 120, p = 0.99. p-values for cell dimension: 10 versus 30 min, p = 0.068; 30 versus 60 min, p = 0.77; 60 versus 90 min, p = 0.003; 90 versus 120 min, p = 0.755. Number of cells for each time are: 10m: 21; 30m: 20; 60m: 24; 90m: 20; 120m: 25. b) Representative immunofluorescence (IF) images of the corresponding YAP/TAZ subcellular localization in U2OS cells. Staining shows nuclei (in blue), YAP/TAZ (in green), and F-actin (in red).

(Figure 11), suggesting that mechanosensing occurs independently of the whole cell shape, and that the formation of initial adhesions and nuclear spreading are the fundamental steps for rigidity sensing, independently and anticipating cell spreading. Indeed, recent work in the literature show how substrates of different stiffnesses can induce changes in nuclear shape, and thus promote nuclear entry of YAP/TAZ, however in these experiments the hydrogel substrate having lowest stiffness still resulted in YAP/TAZ nuclear localization[80].

In order to monitor the impact of substrate stiffness on the shape of the nucleus, and how this effect can be affected by changes in cell ligand density, we analyzed confocal images of the nuclei of U2OS cells plated on the PEG substrate. We found that these cells were sensitive the substrate mechanics through nuclear spreading: we followed two nuclear shape parameters: nuclear height, quantified by

z-stack measurements of the distance between basal and dorsal surfaces of the nucleus (Figure 12), and nuclear spreading, quantified as the Nuclear Projected Area (NPA) (Figure 13).

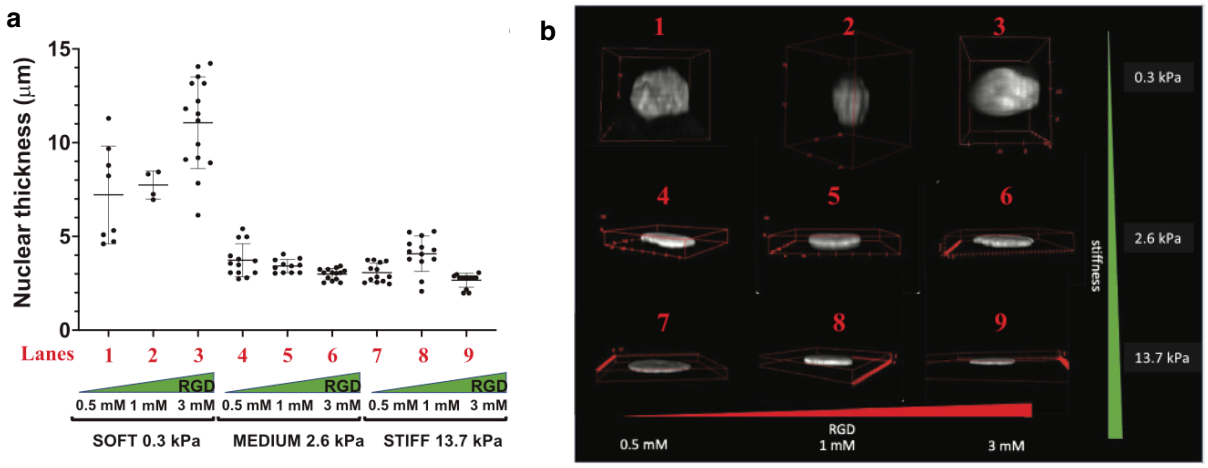

Figure 12: (a) Nuclear thickness of U2OS cells plated on PEG-RGD hydrogels at three different values of stiffness and RGD concentration, number of cells lane 1: 8; lane 2: 4; lane 3: 15; lane 4: 13; lane 5: 11; lane 6: 14; lane 7: 13; lane 8: 13; and lane 9: 13. (b) representative 3D reconstructions of nuclear shapes of U2OS seeded on PEG-RGD hydrogels.

We observed that, while nuclear height sharply dropped upon mechanical activation, for both medium and high stiffnesses and independently of cell adhesiveness, the NPA remained constant at around 100

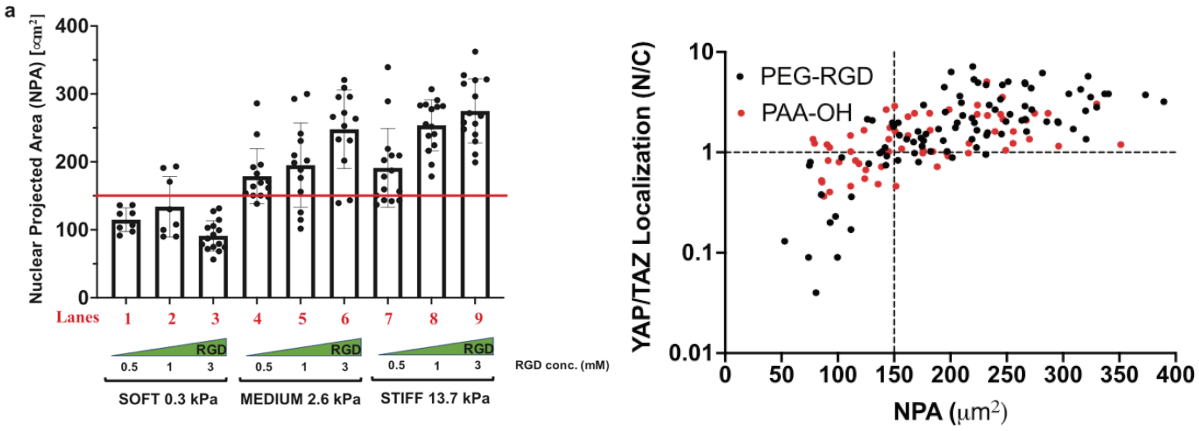

Figure 13: (left) Nuclear thickness of U2OS cells plated on PEG-RGD hydrogels at three different values of stiffness and RGD concentration, number of cells lane 1: 8; lane 2: 8; lane 3: 15; lane 4: 14; lane 5: 13; lane 6: 13; lane 7: 15; lane 8: 15; lane 9: 15 (right) YAP/TAZ Nuclear/Cytoplasmic ratio (N/C) measured for indi- vidual U2OS cells (plated on PEG-RGD and PAA-OH hydrogels with dif- ferent values of stiffness and RGD concentration) as a function of their individual Nuclear Projected Area (NPA). Black dashed line at N/C = 1 give an indication of cells with even YAP/TAZ localization and at NPA = 150 μm2 indicates a threshold for the efficient activation of YAP/TAZ. Sta- tistical significance for monotonic correlation between N/C and NPA was evaluated by Spearman's correlation analysis using 95% as confidence in- terval ($r_s = 0.7277$, $p < 0.0001$ and $r_s = 0.5337$, $p < 0.0001$ for PEG-RGD and PAA-OH, respectively). The number of total cells analyzed is 153.

μm2 on soft hydrogels at all values of RGD concentration. Conversely, the NPA was maximal (270 μm2) on the stiffer substrates (13.7 kPa) and 3mM RGD concentration. Interestingly, the NPA was sensitive to changes in RGD concentration, and ranged between 180 and 240 μm^2 on substrates at intermediate rigidities.

These results, together with the YAP/TAZ localization data, pointed at a threshold for YAP/TAZ activation for NPA of 150 μm^2, placing this shape parameter as a potential permissive checkpoint for YAP/TAZ nuclear entry. To confirm this, we collected the YAP/TAZ N/C values of individual U2OS cells, plated on both PAA-OH and PEG-RGD substrates, as a function of NPA (Figure 13a). A clear correlation emerges between the NPA and YAP/TAZ localization, with most cells surpassing the value of 150um to achieve nuclear localization, independently from the substrate chemistry (Figure 13b).

DPAA (Dynamic PAA-RGD hydrogels)

How cells adjust their tensional state and mechanotrasduction events to substrate stiffness has been so far mainly investigated using different substrates of fixed rigidities: cell-culture plastic, stiff hydrogels, micro-nanopillars. In these studies, cells are dethatched from tissue culture plastic and seeded on the different substrates having defined stiffness[4,28,69,193].

The various structural elements of the cell are inhibited through genetic manipulation of mechanosensitive proteins (an example being talin ablation or mutation of its binding domains)[89] or pharmacological methods (inhibitory and agonist antibodies or small molecules), in order to correlate cell traction and mechanosensing with $\alpha_5\beta_1$ integrins[27] or actin cap fibers and associated perinuclear adhesions[85].

Therefore, while there exist considerable evidences regarding the assembly of the cell tension elements on static substrates, or the effects of external forces[60], information about their response to a variation in mechanical cues is lacking.

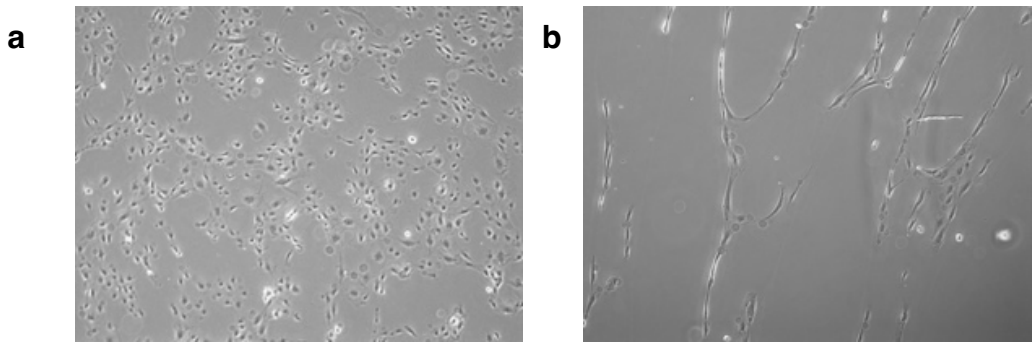

Figure 14: bright-field microscope images of cells seeded on the PAA-OH gels modified with BAC crosslinker, a) before GSH treatment b) after addition of GSH

To fill this gap, we developed a hydrogel material responsive to a mild, cytocompatible trigger for softening: glutathione (GSH), a key component of the endogenous antioxidant system of the cell. Glutathione levels in the cytosol of mammalian cells are reported in the millimolar range (1-10mM)[191] and it is a common component of cell culture media as a protecting agent from oxidative stress[194].To achieve softening using GSH, we introduced disulfide crosslinks in PAA hydrogels by using N,N'-Bis(acryloyl)cystamine (BAC), a commercially available and disulfide containing analogue of BA that has been used to prepare thiol-dissolvable gels for electrophoretic separations[195].

We first attempted this approach for FN coated PAA-OH hydrogels, by substituting a significant amount of BA with BAC (>70% w/w), however the coating procedure was incompatible with this softening strategy, as upon adding the GSH containing medium the protein coating detached from the gel surface, producing bundles of fibers and cell detachment (Figure 14).

To overcome the limitations posed by the protein coating, we opted for a chemistry similar to the PAA-RGD system: by using variable monomer concentrations of AA, BA and BAC, gels with different starting stiffnesses were obtained (Table 5, Figure 16).

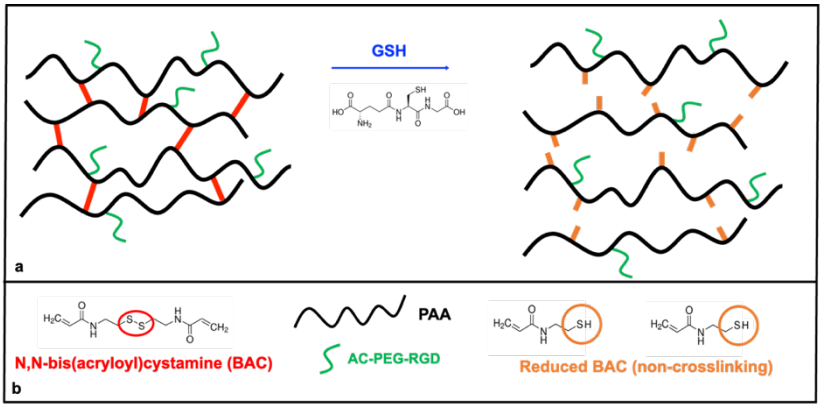

Figure 15: schematic representation of the DPAA hydrogels structure and the GSH mediated softening process

Table 5: monomer compositions of the prepared DPAA hydrogels and corresponding elastic moduli measurements collected with the micropipette aspiration method before the softening process (E_{in}) and after 1h of treatment (E_{fin}) using different concentrations of GSH

Degradable DPAA gel compositions		**Initial and final stiffness (kPa) after GSH degradation for 1h**		
%AA	**%BAC**	**E_{in}**	**E_{fin} 10mM$_{GHS}$**	**E_{fin} 1mM$_{GHS}$**
5	0.1	2.80 ± 0.17	-	0.29 ± 0.05
5	0.2	3.93 ± 0.49	-	0.85 ± 0.20
5	0.3	4.67 ± 0.38	-	1.35 ±0.11
5	0.4	6.6±0.46	-	4.09 ± 0.20
7	0.1	3.83 ± 0.35	0.004 ± 0.001	0.43 ± 0.14
7	0.15	6.02 ± 0.45	0.07 ± 0.02	-
7	0.2	7.41 ± 0.10	0.10 ± 0.03	-
7	0.3	12.23 ± 0.45	0.50 ± 0.05	1.86 ± 0.17
7	0.48	19.08 ± 0.84	3.14 ± 0.400	-

Elastic modulus measurements were carried out by micropipette aspiration during the softening process in culture medium supplemented with 1mM GSH, to assess the degradation process: the elastic modulus gradually decreased when placing the hydrogels, over the course of about 1-2h, a timescale compatible with live-cell imaging and PFA fixation at defined timepoints (Figure 17).

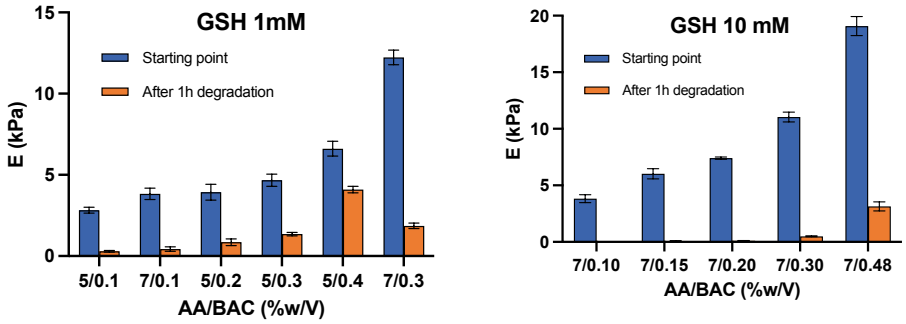

Figure 16:elastic moduli of gels prepared with an AA concentration of 7% or 5% and variable BAC amount after 24h equilibration in PBS (blue) and softened in 1h with 1mM (a) or 10mM (b) of GSH (orange)

Although for all of the prepared hydrogel compositions the total amount of GSH added was in stoichiometric excess with respect to the disulfide bonds, dissolution was not observed, so we investigated the effect of higher amounts of GSH and longer exposure times.

Indeed, full degradation of the gels was observed, for lightly crosslinked hydrogels (<0.3% BAC) with 1h exposure in 10mM GSH. Conversely, gels with a higher amount of crosslinker resisted exposure up to 2h with a measurable elastic modulus (Figure 16), suggesting the presence of cross-links that are not susceptible to GSH reduction, such as polymer entanglements, or partial oxidation of GSH in the softening medium from dissolved oxygen.

We also verified whether the process could be reversed by washing the medium and adding oxidized glutathione (GSSG) to a softened substrate, but no effect on the gel stiffness was obtained. Possibly,

the thiol groups in the reduced network are brought too far apart to establish elastically effective crosslinks after swelling.

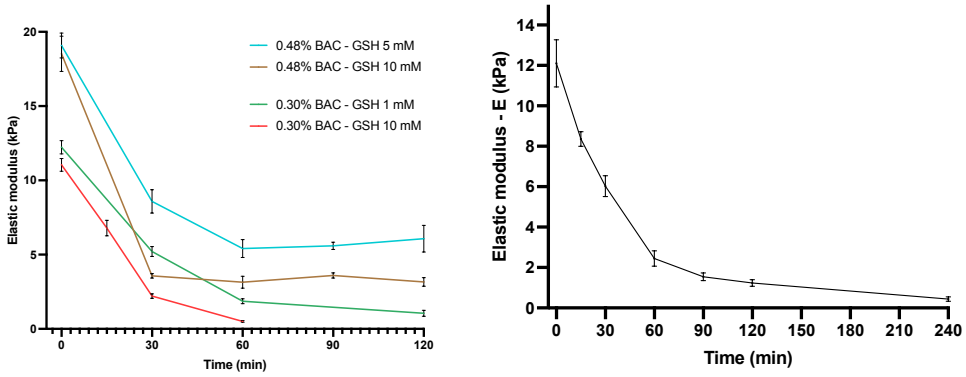

Figure 17: Results on softening experiments made on degradable gels with two formulations and initial stiffnesses (7%AA and 0.48 or 0.3% BAC) and different GSH concentrations. The degradation has been followed until a plateau value of stiffness is reached. Depending on the amount of GSH the degradation rate ranges from some minutes to a couple of hours. The formulations of all gels are reported in Table I. (d) Softening of degradable gel used for the seeding experiments.

Then, we conducted AFM measurements to assess whether the stiffness at the very surface of the gels, which is directly perceived by cells, follows the same changes as the bulk material, as measured by micropipette aspiration.

First, we verified if the polymerization conditions lead to uniform mechanical properties of the gel surface and the bulk material. By casting the gels against different substrates (Kapton plastic or glass slides), we found that when Kapton slides were used, oxygen diffusion from the plastic film inhibited the polymerization at the gel surface[196], leading to lowered surface stiffness compared to the hydrogel bulk (Table 6).

Table 6: elastic moduli for two DPAA hydrogel composition, as measured through a surface-sensitive method (AFM indentation) and a material bulk-sensitive one (micropipette aspiration)

%AA - %BA	Bulk E / plastic	Bulk E / glass	Sup. E / plastic	Sup. E / glass
7 – 0.1	2 kPa	2 kPa	65 Pa	2 kPa
7 – 0.3	10 kPa	10 kPa	600Pa	10 kPa

We then measured the elastic modulus of the surface during the softening process, to assess whether a stiffness gradient is realized or rather the gel is homogenously softened throughout its thickness. From the results (Figure 18) the surface and bulk elasticity of the material, as measured by AFM and micropipette aspiration respectively, are comparable throughout the process, considering the different accuracies of the two techniques[197]. It follows that GSH can quickly react and diffuse through the material leading to a uniform softening process.

To ensure that the swelling process did not distort the hydrogel during 1mM GSH softening, the behavior of the surface of the gel was assessed by embedding fluorescent nanoparticles and imaging them through confocal microscopy. While there was significant vertical swelling (Figure 19), the fact that the hydrogels are bound to the coverslip, effectively prevented lateral swelling, as distances between particles were constant (Figure 19), this is a critical feature of the system as it guarantees that the surface distribution of integrin ligands remains constant during the softening process.

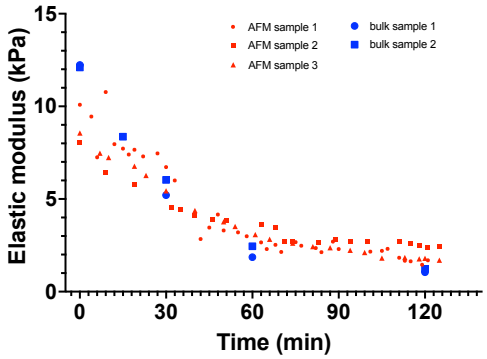

Figure 18: stiffness measurements conducted during the softening process mediated by 1mM GSH on 0.3%BAC hydrogel, micropipette measurements are reported in the graph as blue symbols and AFM measurements as red symbols.

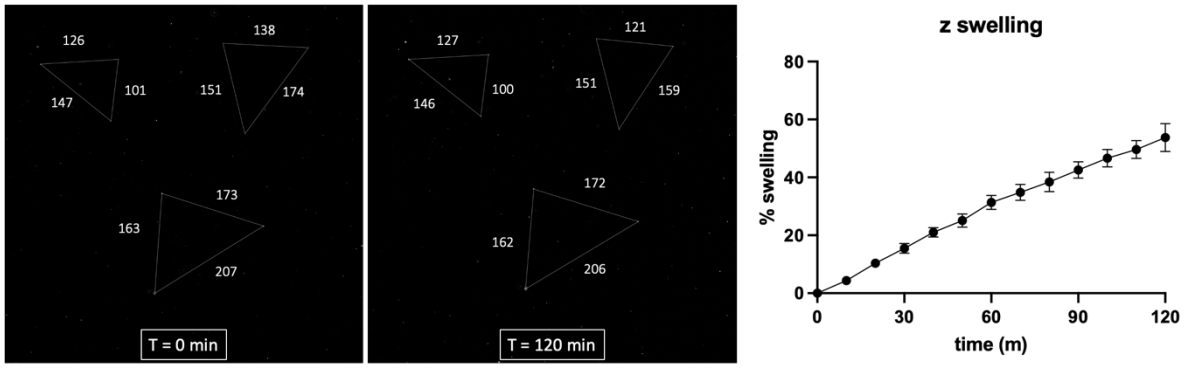

Figure 19: (left) confocal images displaying the relative positions (in micrometers) of fluorescent beads embedded on the surface of a DPAA hydrogel before (T = 0 min) and after (T = 120 min) 10mM GSH mediated softening (right) hydrogel volumetric swelling monitored during the softening process by recording the focal plane height during the process.

As fibroblasts have been shown to be responsive to changes in substrate stiffness by reorganizing their cytoskeleton, we investigated the effect of these dynamic substrates on Wi38 cells.

As a reference, Wi38 cells were plated on static gels, with stiffnesses ranging from 0.3 to 30 kPa, and we monitored their cytoskeletal morphology and YAP/TAZ localization on the substrates (Figure 20).

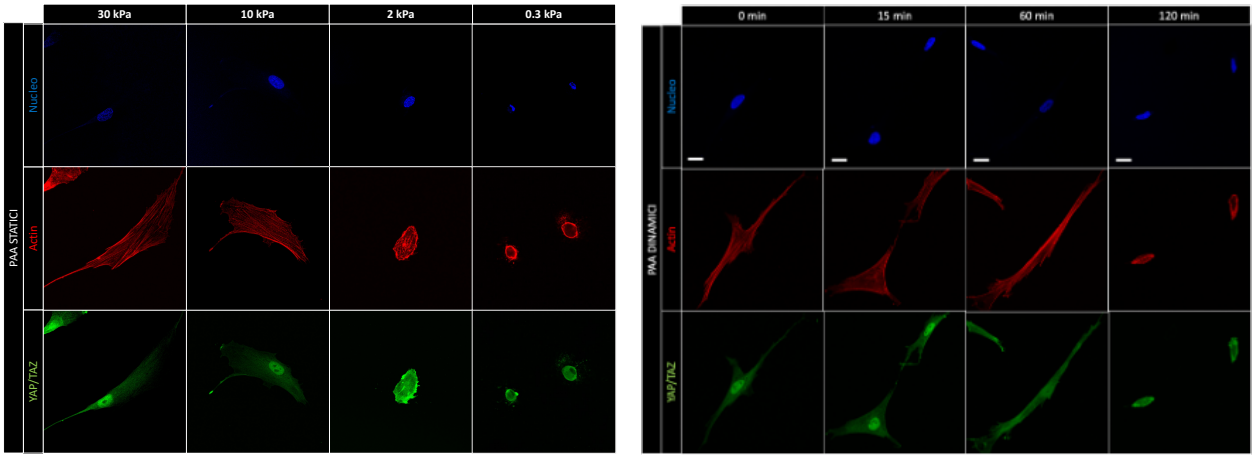

Figure 20:representative IF images of Wi38 fibroblasts seeded on PAA-RGD hydrogels with static elasticity (left) and fixed at defined timepoints on DPAA hydrogels during the softening process with 1mM GSH (right). Nuclear DNA signal is reported in blue, F-actin in red, and YAP/TAZ in green.

Cells were fully spread on the stiffer substrates and exhibited a dramatic transition towards a rounded shape occurring between 10kPa and 0.3 kPa. Following a similar trend, YAP/TAZ localization shifted from prevalently nuclear on the 30 kPa substrates, towards a fully cytoplasmic localization on soft substrates < 0.3 kPa. (Figure 20)

Having defined a stiffness range of interest, as Wi38 fibroblasts exhibited the most relevant differences between static gels at 10kPa and 2kPa, we observed the response of these cells to a gradual suppression of mechanical cues, by plating Wi38 cells on DPAA gels with initial and final stiffness of about 12kPa and 1kPa respectively. The cells response was followed by processing the samples for

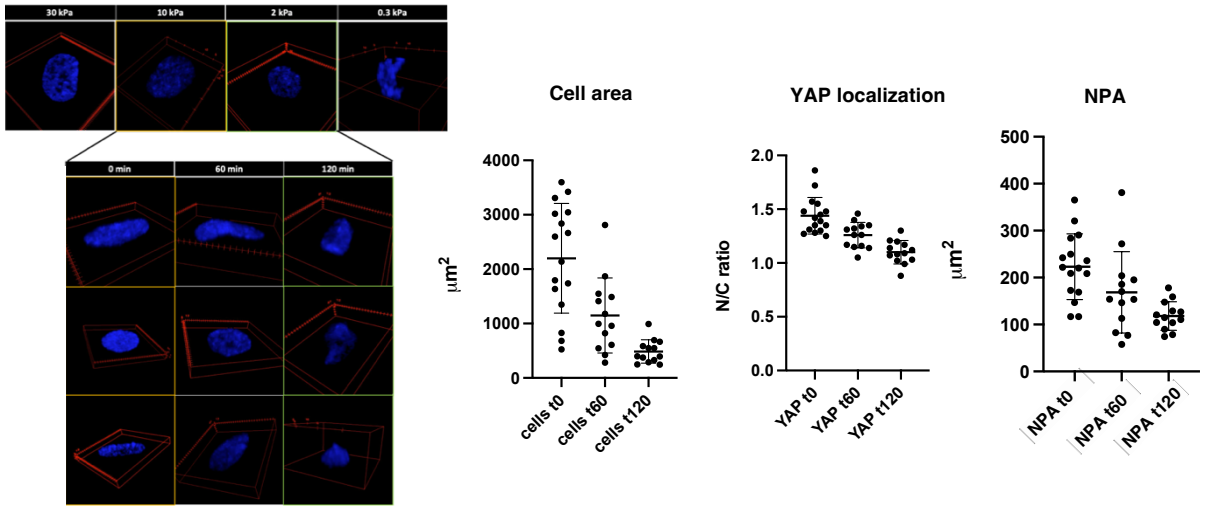

Figure 21: (left) representative 3D reconstructions of the nuclear shape of Wi38 cells seeded on static PAA-RGD hydrogels, from stacking of confocal images of the nuclei stained with Hoechst 33342 (top) and DPAA hydrogels during softening (bottom). (right) cell shape parameters quantified at the starting timepoint (t0) and 1h (t60) and 2h (t120) timepoints.

immunofluorescence after PFA fixation at defined timepoints, over an interval of 2h. (Figure 20).

During the softening process, cells quickly responded to gradual stiffness changes by adapting their shape (as quantified by the cytoskeletal area Figure 20, Figure 21). However, up to 60 min softening corresponding to E = 2kPa, cells preserved the orientation of their actin cytoskeleton (major axis length) and most cells still displayed actin cap fibers, aligned with the major axis of the cell. Accordingly, while a discrete increase in NPA is observed during the first hour, the actin cap still preserves a flat nuclear shape (Figure 21). This is markedly different from the behavior of cells plated on static gels with comparable stiffness.

After an additional hour of softening elapsed, with the substrate approaching a 1kPa elastic modulus, the cell structure further adapts, and while cell area significantly lowers, the cytoskeleton still displays a weak elongation, and a limited number of actin cap fibers are observable. Differently from the cytoskeletal area, the NPA is only marginally reduced, along with YAP/TAZ localization (Figure 21). Consistently with the behavior of cells seeded on PEG-RGD hydrogels at early timepoints, these observations support the hypothesis that cell mechanoresponse occurs independently from cell spreading.

Fibroblasts express two major integrin dimers that recognize the RGD sequence: $\alpha_5\beta_1$ (also termed the fibronectin receptor) and $\alpha_v\beta_3$ (the vitronectin receptor), and studies attribute distinct localization and force generation[8], or roles in establishing adhesion force and mechanosensing to the two subtypes[27]. Observations on fibroblasts seeded on lipid-membrane bound RGD, that are able to translocate laterally and do not allow to develop actomyosin contractility, revealed that RGD ligands were able to activate both β_1 and β_3 integrins, however clusters of β_3 integrins required establishment of tension (glass-bound RGD) for maturation, and were otherwise targeted for endocytosis[198]

We observed the localization and shape of the adhesions containing the two integrins by IF staining (Figure 22). Cells displayed adhesions containing the RGD specific integrins αvβ3 and α5β1 in both the static and DPAA hydrogels throughout the softening experiments, confirming that the change in morphology is due to the cell response to a lowered elastic modulus and not to a loss of cell-adhesive moieties of the substrate. While on stiff (30kPa) static gels both $\alpha_v\beta_3$ and $\alpha_5\beta_1$ integrin types are localized in elongated FA, β_1 containing adhesions are present at a higher density in the perinuclear region as punctiform spots.

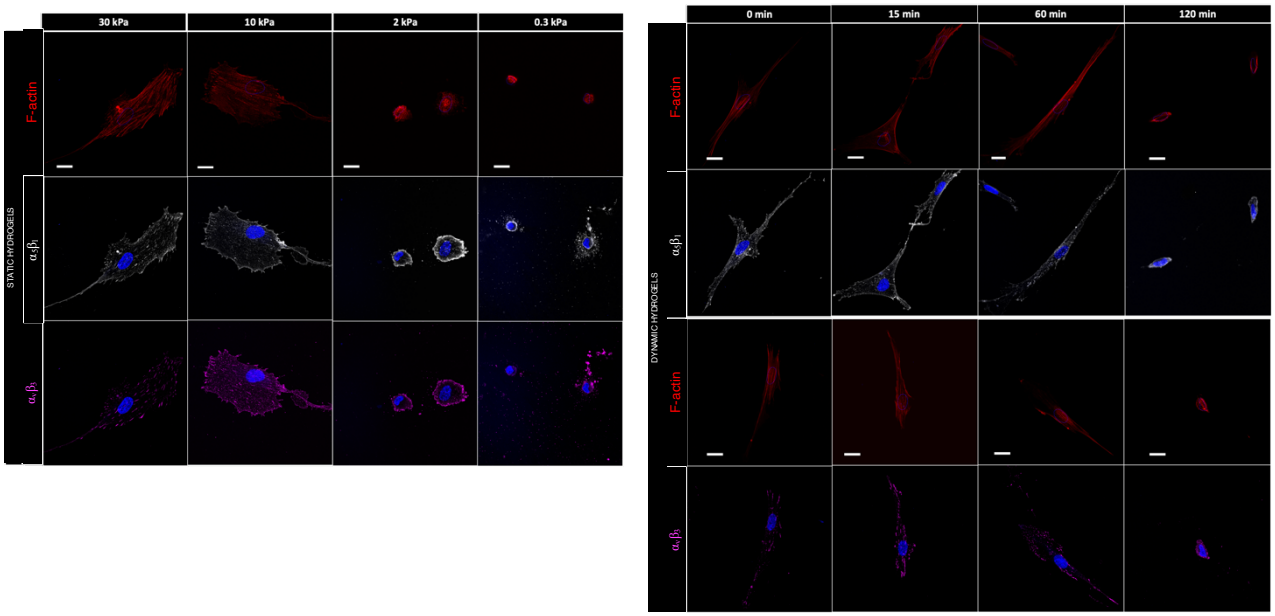

Figure 22:representative IF images of Wi38 cells seeded on PAA-RGD hydrogels (left) and on DPAA substrate fixed at defined timepoints after adding 1mM GSH medium (right). Nuclear DNA signal is reported in blue, F-actin in red, $\alpha_5\beta_1$ integrins in white and $\alpha_v\beta_3$ integrins in purple.

Role of YAP/TAZ as determinant of nuclear integrity and in turn control of cell senescence.

In experiments shown in Figure 13 above, we showed how dosing mechanical cues using defined hydrogels impacts on nuclear shape. Cells in a YAP ON, mechano-activated state, display a flattened nucleus (Fig 13b 6-9). Instead, mechanically inhibited cells, that is cells in a YAP OFF state, display a progressively increased nuclear thickness, blebbing and wrinkling. But is there a causative, mechanistic connection between the YAP ON vs OFF state and nuclear shape? And, if so, what are the phenotypic consequences at the cell biology level of this connection? During my PhD I contributed to a paper that addressed these questions in the context of a broad theme, that is, how YAP mechanosignaling prevents aging[199]. The main conclusion from that work is that YAP/TAZ mechanotransduction plays an active role at preserving the integrity of nuclear envelope by controlling organization of the perinuclear set of special F-actin filaments, termed the actin-cap[200], and expression of Lamin B1, a main component of the nuclear envelope[76]. The actin cap is, in fibroblasts, what controls the shape of the nucleus: it represents a dome-like structure of F-actin filaments that wraps around the apical surface of the nucleus, anchoring it to integrins on the basal surface of cells, as such keeping the NE smoothly distended and preventing its deformation[201,202]. Actin cap filaments directly connect to the NE, in part through LINC complexes[202] and end to specialized focal adhesions on the cell basal surface[203]. Interestingly, the actin cap and its nuclear shape-determining functions are lost in

lamin-deficient fibroblasts, such as in progeria[202]. Work led by Hanna Sladitschek in our laboratory showed that loss of YAP/TAZ in mechano-OFF cells causes cells to lose ARP2/3, a direct transcriptional target of YAP/TAZ, and this loss is what causes loss of the actin-cap and increased nuclear thickness. We further discovered that these nuclear dysmorphologies were followed by cGAS activation and transcription of SASP markers. cGAS is a sensor of cytoplasmic DNA, induced by viral infection of by the rupture of the NE, in turn causing spill-over of nuclear DNA in the cytoplasm. cGAS is a leading inducer of cellular senescence (Figure 23).

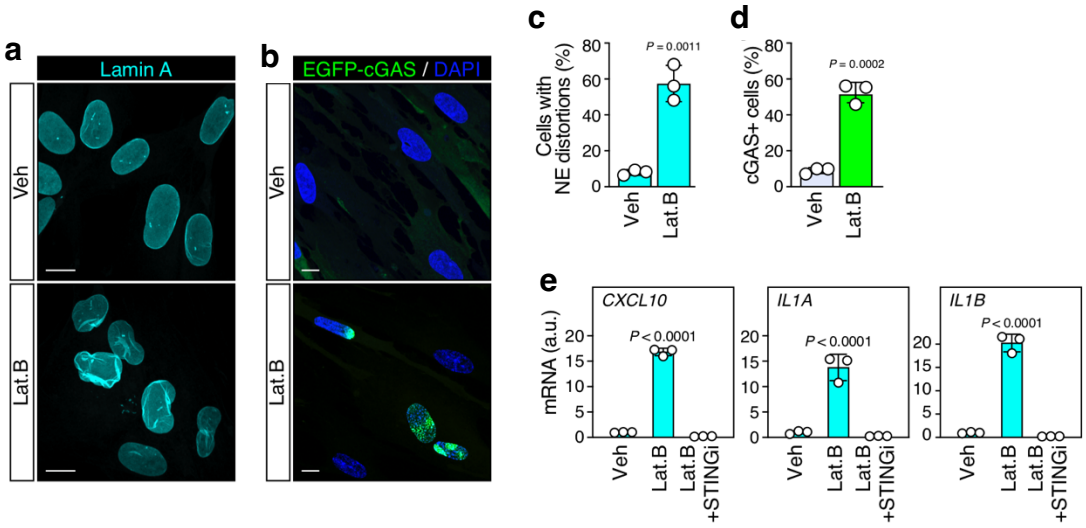

Figure 23: Role of YAP/TAZ in maintaining nuclear morphology and actin cap architecture. a) Nuclear morphology of WI-38 cells treated with 0.1 µm Lat.B (2 hours) or Vehicle (Veh) visualized by Lamin A immunostaining (bar=10 µm). c) Quantifications of phenotypes shown in panels a-b, presented as mean ± s.d.; P values are derived from unpaired t-test, e) RT-qPCR analysis of SASP marker genes in WI-38 upon treatment with 0.1 µM Latrunculin B (Lat.B, 5 hours) with or without concomitant STING inhibition (STINGi, 1 µM H-151). Data are shown as mean ± s.d.; P values are derived from one-way ANOVA with Dunnett's multiple comparison test.

This work thus offered direct evidence that YAP/TAZ mechanotransduction in stromal cells of adult organs is crucial to keep senescence at bay, and suggests that YAP/TAZ biology in these cell types may serve as primary target of future efforts to interfere with aging. My contribution to the above work has been the generation of soft hydrogels for YAP/TAZ and cGAS/STING mechanobiology assays.

Mechano-activation of YAP/TAZ protects the nucleus from damage caused by mechanical strains

As unpublished evidence that we find appropriate to mention as ongoing follow up work, we considered that high levels of mechanical deformations, such as cell pulling-and-squeezing, can

themselves induce tearing of the nuclear envelope[203]. With this background in mind, we considered to expose primary fibroblasts to an extended series of mechanical deformations by plating them as confluent monolayers on fibronectin-coated PDMS membranes and subjecting these cells to a regimen of 0.5 Hz cyclic stretching-and-recoil over 2 hours (Fig. 5k). To carry out these experiments, we used a stretching device (MCB1, CellScale) applying a controlled biaxial stretch and recovery to a PDMS membrane covalently functionalized with fibronectin.

In order to avoid artefacts due to uneven distribution of the cell-adhesive protein, we adjusted the functionalization protocol, in particular the concentration of the fibronectin solution, to achieve uniform functionalization of the membranes, as assessed by IF staining (Figure 24)

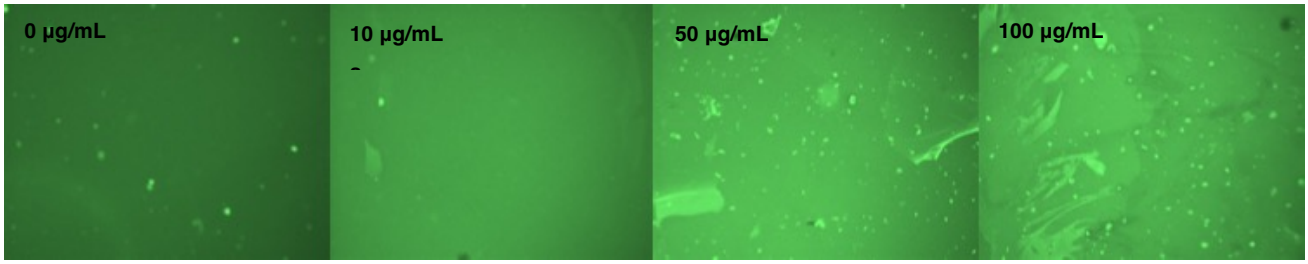

Figure 24: representative epifluorescence images of PDMS membranes functionalized by incubation in PBS buffer with different concentrations of fibronectin

We found that these mechanical strains had only limited effects on activation of cGAS/STING signaling in control cells (Figure 25).

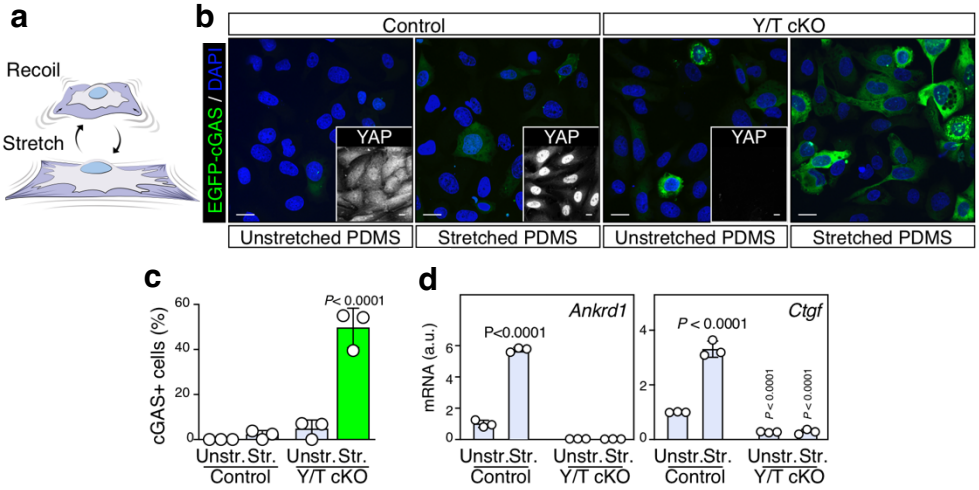

Figure 25: a) schematic representation of the cell-stretching experiments b) EGFP-cGAS reporter signal in control and YAP/TAZ cKO primary MAFs plated on PDMS membranes, either left unstretched or after 2 hours of stretch-recoil cycles. Insets are immunostaining for YAP. Note nuclear accumulation of YAP upon stretching (bar=10 µm) c) quantification of control and Y/T cKO MAFs displaying EGFP-cGAS reporter activation in resting state (Unstr.) or after 2 hours of cyclic stretching (Str.) (n=3) d) RT-qPCR analysis of the YAP/TAZ target genes in MAFs, either unstretched (Unstr.) or after 2 hours of cyclic stretching (Str.). Genetic ablation of YAP/TAZ serves as specificity control of YAP/TAZ activation by stretching (n=3).

However, we noticed that this regime also triggered massive YAP/TAZ nuclear accumulation and activation (Figure 25 b), in line with the possibility that this may in fact imbue protection from such

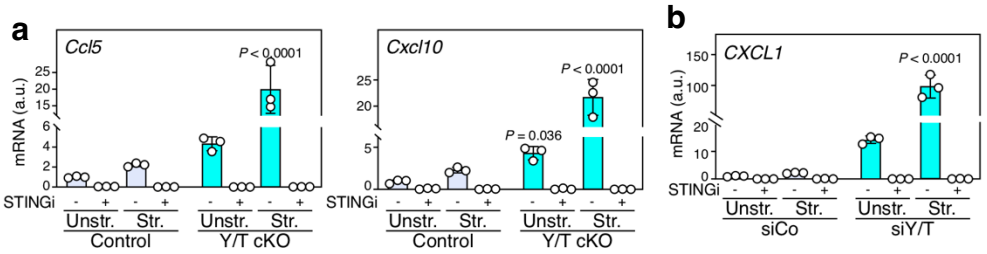

Figure 26: RT-qPCR analysis of SASP marker gene expression in primary MAFs (a) or in WI-38 cells (b) after depletion of YAP/TAZ, either left unstretched or after 2 hours of cyclic stretch, in absence or presence of STING inhibitor (STINGi, 1µM H-151) (n=3).

repeated mechanical strains. To address this, we tested the effects of cyclic stretching on YAP/TAZ knockout cells in both MAF and WI-38 fibroblasts, finding dramatic upregulation of cGAS and SASP expression (Figure 25 c, Figure 26).

Thus, an excess of mechanical strain has the potential to induce cell senescence, but the concomitant activation of YAP/TAZ prevents this event. This configures YAP/TAZ as elements of a feedback loop by which their activation by mechanical stimulations in stromal cells in fact shields from the potentially harmful effects of the same mechanical forces.

DISCUSSION AND PERSPECTIVES

In this work, we developed and optimized diverse hydrogel systems as supports for mechanobiology studies and validated the mechanical response of different cell lines through YAP/TAZ, two transcriptional regulators functioning as a molecular beacon of cell mechanotransduction[12].

In this framework, an easily scalable fabrication method based on hydroxyl-functionalized polyacrylamide hydrogels (PAA-OH) was developed to present cells with culture substrates with defined stiffness and full-length cell adhesive proteins. Then, a fully synthetic matrix, PEG-RGD, was prepared, to decouple the contributions of hydrogel stiffness and density of cell-adhesive island to determine the mechanical response of cells.

Furthermore, since in living tissues cells continuously adapt their structure their mechanochemical environment, materials that allow in situ tuning in their surface properties are needed to better mimic the continuous changes in physical signals occurring in both normal physiology (blood flow, muscle contraction) and during development, tissue repair or disease states[204].

To address this, we developed a dynamic hydrogel system, DPAA, that enables controllable and tunable decrease in substrate stiffness, and observe the resulting cell response through YAP/TAZ localization during the process. We also followed the disassembly of the key mechanosensitive cytoskeletal structures, focal adhesions and actin cap stress fibers in fibroblasts.

The hydrogel systems developed in this work were optimized to be applied for cell mechanotransduction studies, using YAP/TAZ as proxy of the cell response induced by the substrate physical properties, guiding the process of developing the materials. This approach to biomaterial design does not constitute the norm in the field, where typically materials are first designed and characterized for their physicochemical features, and then assayed in their application with cells, often dispensing of analyzing YAP/TAZ activity[171,174,188,192,205]. In particular, the application of substrate softening to observe the disassembly of key structural elements of the cell, while preserving the components of the initial tensegrity architecture, constitutes a novel approach with respect of recent studies in the field, that rely instead on disruption of mechanosensitive proteins or cell contractility to evaluate their contribution to the mechanoresponse of the cell[27,40,85,89]. This work thus addresses the lack of insights about the response of the load-bearing elements of the cell induced by decreasing the mechanical stimuli originating from the ECM.

Static hydrogels

In order to develop a streamlined and scalable protocol for the fabrication of substrates for stiffness assays in mechanobiology, we optimized the polymerization and functionalization of PAA-OH hydrogels with fibronectin. By monitoring YAP/TAZ activity of cells seeded on the PAA-OH hydrogels, we optimized the system under two key aspects: first and foremost, the efficacy of the materials in providing a full range of adhesive and mechanical cues to cell, capable of eliciting a spectrum of mechanotransduction responses, from fully inactivating (cytoplasmic YAP) to activating (nuclear YAP) was confirmed. Secondly, we were able to address a critical aspect of the fabrication procedure (the extent of surface drying) and found that the functionalization procedure was also applicable to another ECM protein, laminin.

In an ideal advancement with respect to PAA-OH, the synthesis of PEG-RGD hydrogels provided fully defined substrates, obviating the drawbacks derived from full-length protein functionalization, and allowed precise and independent control over the rigidity and concentration of adhesive cues. This platform revealed how the substrate stiffness constitutes a prevailing input governing YAP/TAZ activity, while increasing the amount cell-adhesive cues plays a modulating role, impacting mechanosensing at intermediate rigidities.

The combined measurements of nuclear morphology and YAP/TAZ activity of U2OS cells seeded on all the compositions of PAA-OH and PEG-RGD hydrogels, revealed the role of nuclear shape as a mediator of the mechanotransduction response, irrespectively of substrate chemistry, and contributed to define a threshold of NPA (150 μm^2) that cells need to surpass to attain YAP/TAZ nuclear entry.

Dynamic hydrogels

With the objective of obtaining a dynamic cell culture substrate, allowing control of softening in a range of time and stiffnesses compatible with a gradual adaptation of cells, we developed the GSH-responsive DPAA hydrogels. The system allows variations in the range of starting and final stiffness, by changing the amounts of AA monomer and BAC crosslinker in the polymerization solution, furthermore, the timing of the softening process is readily tunable by changing the concentration of GSH in the medium. The softening procedure is homogeneous across the material, and does not affect the surface distribution of cell-adhesive moieties on the hydrogel surface.

By prolonged exposure to 10mM GSH, hydrogels with lower BAC concentrations were fully degraded, however for the same materials, after 1 mM GSH was used, a gel with measurable elastic modulus

was obtained, thus allowing the application of these substrate in a softening experiment and processing the hydrogels for immunofluorescence at defined timepoints.

Perspectives

As a possible development to the DPAA platform, a substrate allowing controllable stiffening would be interesting under two main aspects: such a system would allow to observing YAP entry and assembly of cytoskeletal structures and would be relevant for model tissue stiffening in pathologies such as fibrosis and cancer.

The swelling of the DPAA substrates during softening represents a complication for live-cell imaging, as the plane of focus needs to follow the rising hydrogel plane, a possible development of the system could involve minimizing this effect. Approaches to attain hydrogel degradation with minimal swelling have been explored in the literature, by tuning the solvent interaction parameters of the polymer chains[206] however, this strategy would require the dedicated synthesis of modified precursors, thus limiting the ease of access of the fabrication protocol.

METHODS

Reagents and Plasmids

Fetal bovine serum (10270-106), L-glutamine (25030-024), Pen/Strep (15140-122), DMEM/F12 (11320-074), DMEM (41965-039), MEM (31095-029), trypsin-EDTA 0.05% (25300-054), H-151 (SML2437) were from Sigma-Aldrich. Latrunculin B was from Cayman (Item No. 10010631).

The pCW57.1-YAP5SA vector was generated by subcloning YAP5SA into the pCW57.1 vector (Addgene #41393). pTRIP-EF1a-EGFP-Flag-Cgas E225A-D227A was cloned by substituting the CMV promoter of pTRIP-CMV-EGFP-Flag-Cgas E225A-D227A vector (AddGene #86674) with the EF1a promoter from the MXS_EF1a vector (AddGene #62421) via MluI/SalI. All constructs were confirmed by sequencing.

Cell lines, treatments and transfections

MCF10A human mammary epithelial cells were maintained in DMEM/F12 medium, with 5% horse serum, l-glutamine and antibiotics and freshly supplemented with 20 ng/mL epidermal growth factor (EGF), 0.5 mg/mL hydrocortisone, 100 ng/mL cholera toxin,10 μg/mL insulin, and 1% (v/v) penicillin-streptomycin (P/S).

U2OS human osteosarcoma cells were maintained in DMEM, supplemented with 10% FBS, l-glutamine and P/S.

WI-38 human fibroblasts were maintained in MEM, supplemented with 10% FBS, l-glutamine and P/S.

Primary mouse adult fibroblasts (MAFs) were isolated from biopsies of dorsal skin. Briefly, tissue was minced and digested in Collagenase, Type I (2000U/ml in PBS - Thermo Fisher Scientific, CAS No. 9001-12-1) for 1 hour at 37°C, with vigorous shaking. Samples were filtered through a 70 μm cell strainer, plated on 0.2% gelatin-coated dish and maintained in DMEM-F12 medium, supplemented with 20% Fetal Bovine Serum (FBS), L-Glutamine and antibiotics.

For in vitro YAP overexpression studies in WI-38 fibroblasts, cells were transduced with the lentiviral pCW57.1-YAP5SA vector (or empty pCW57.1 vector as control) and maintained in the presence of 10 μg/ml Doxycycline hyclate (Sigma-Aldrich, D9891) for 36 hours. For EGFP-cGAS reporter studies on primary MAFs and WI-38 fibroblasts, cells were transduced with the lentiviral pTRIP-EF1a-EGFP-Flag-Cgas E225A-D227A vector. Briefly, cells were brought to single-cell suspension, overlaid with viral supernatant and spun at 7.0 RCF for 1.5 hours.

siRNA transfections in WI-38 fibroblasts were carried out using Lipofectamine RNAi-MAX (Life Technologies, 56532) in antibiotics-free medium according to the manufacturer's instructions. siRNA transfections in primary MAFs were carried out using GenMute siRNA transfection reagents (SignaGen Laboratories, SL100568-SMC) according to the manufacturer's instructions. Cells were harvested 48 hours after siRNA transfection, unless otherwise specified.

Stretching-recoiling experiments

Stretching-recoiling experiments were carried out on a radial cell stretching device (MCB1, Cellscale) applying a cyclic stimulation protocol with a maximum stretch of 10%. The stretching cycle had a period of 2 seconds and consisted of a resting step of 0.25 seconds at the non-stretched position, a stretching ramp of 0.75 seconds from 0% to 10% stretching, a holding step of 0.25 seconds at the maximum stretch and the stretching release in 0.75 seconds from 10% to 0% stretching. This cycle was repeated for 2 hours. The stretching culturing substrates were punched circles of a 150 μm thick Polydimethylsiloxane (PDMS) sheet (SMi Specialty manufacturing inc.). The PDMS membranes were plasma treated in an air plasma cleaner for 90 seconds and silanized with a 10% v/v solution of (3-Aminopropyl)trimethoxysilane (APTMS, Sigma-Aldrich) in pure ethanol. A reaction with a 3% solution of glutaraldehyde in water was then performed for 20 minutes at room temperature. Membranes were covalently functionalized by incubation with 10 μg/mL solution of fibronectin in PBS for 1 hour at 37°C. The PDMS substrates were then washed with a 50 mM solution of glycine in PBS to quench the residual reactive aldehydes, and twice with PBS before cell seeding.

Methacrylate-functionalized glass coverslips

Clean glass coverslips were treated with plasma (Harricks Expanded Plasma Cleaner 230V) and then functionalized by applying a solution of TMSPM (diluted 1:50 with 5%v/v acetic acid in absolute ethanol) for 15 minutes. The treated coverslips were then washed with acetone and air dried.

Non-adhesive glass coverslips

Clean microscope slides were treated with a 1M NaOH solution for 10 minutes, washed three times with milliQ water, once with absolute ethanol and then dried. The slides were then functionalized by applying a dimethyldichlorosilane (Repel-silane ES) solution for 10 minutes, followed by three washes with absolute ethanol and air dried.

PAA-OH hydrogel synthesis

Acrylamide (AA) solution (40% w/v in water), bisacrylamide (BA) solution (2% w/v in water) and water were mixed in the proper ratio to obtain the prepolymer solution. N-hydroxyethyl acrylamide (HEA) was added to a final molar concentration of 0.1M. The solution was then brought to 37°C with a water bath and degassed for 15' at 0.1 bar. Ammonium persulfate (APS) dissolved in water (10% w/v for PAA 1-2 and 20% w/v for PAA 3-6). After degassing, polymerization was initiated by adding 0.1% v/v tetramethylethylenediamine (TEMED) and 1% v/v APS solution to the monomers. The resulting solution was mixed and dispensed in silicone molds and a methacrylated glass coverslip was used to seal the mold. Once polymerized, the gels were detached from the molds and placed in milliQ water.

PAA-OH protein functionalization

Hydrogels were sterilized by UV exposure for 15 min, then they were incubated at 37°C overnight with a 25 ug/mL fibronectin (human plasma, Corning) solution in PBS. Then, gels were extensively washed with sterile PBS to remove excess protein. For laminin (EHS murine sarcoma, Sigma-Aldrich) coating was performed with a 25 ug/mL laminin solution in PBS.
For fluorescence imaging of the fibronectin coating, Alexa Fluor 488 labelled fibrinogen (Thermo Scientific) was added to the coating solution (2ug/mL).
Laminin coating was visualized by immunofluorescence staining. Confocal images were collected immediately after the drying step for fibronectin coated gels and after immunofluorescence staining for laminin, without applying mountant.

PEG-RGD hydrogel synthesis

A previously reported procedure[192] was adapted to obtain hydrogels with an extended range of stiffnesses. The following stock solutions were prepared: 8-arm PEG, norbornene (NB) terminated (40kDa, Creative PEGworks, 250 mg/mL), bi-cysteine terminated synthetic peptides CRDGQPGYSGQDRC (crosslinking peptide, 40mg/mL), mono-cysteine terminated adhesive peptide GRGDSPC (37.5 mg/mL) and GRDGSPC non-adhesive peptide (37.5 mg/mL) and a photoinitiator (Lithium phenyl-2,4,6- trimethylbenzoylphosphinate, LAP, 31.7mg/mL). The stock solutions were mixed obtain the final PEG concentrations and molar ratios between NB functionalities and the cysteine terminal groups of the crosslinking peptide reported in Table 3. For all compositions GRGDSPC has a concentration in the final gel volume of 0.5, 1 or 3mM. The non-adhesive peptide

GRDGSPC was added to have a total concentration of mono-cysteine terminated peptides of 3mM for each composition. LAP was added to a concentration of 1% w/w respect to PEG. All peptides were supplied by CRIBI Biotechnology Center, University of Padova.

Molds for polymerization were assembled by arranging circular gaskets of PDMS (250μm thick, diameter 22mm) on a cleaned and plasma treated glass coverslips. A 40 μL drop of the precursor solution was poured in each gasket. An adhesive functionalized glass coverslip was then placed on top of the solution to homogeneously spread the drop and facilitate handling the hydrogels.

The solutions were then exposed under a UV led light (Delolux 20) with the emission peak centered at 400 nm. The light dose was dependent on the gel composition used: 10 min exposure at 65 mW/cm^2 or 2 min exposure at 26 mW/cm^2 for the softer (PEG-RGD 1- 4) and stiffer (PEG-RGD 5 and 6) gel respectively. After polymerization, the gels were removed from the mold and were left in PBS overnight to reach swelling equilibrium.

PAA-RGD hydrogel synthesis / Dynamic PAA hydrogels synthesis

N,N-Bis(acryloyl)cystamine (BAC) was dissolved in 40% AA solution to a final 3% w/v concentration of BAC. APS was dissolved 10% w/v in water. Acrylate-PEG-maleimide (Laysan Bio, MW 5000) was conjugated with a cysteine terminated peptide containing the cell adhesive motif RGD (GRGDSPC): the reaction was performed in water at room temperature for 20 min, with a 1.1-fold molar excess of the peptide to a final 10% w/v concentration. The functionalized PEG monomer was used without further purification by mixing with AA solution (40%), BA solution (2%), BAC solution and water in the proper ratio to obtain the prepolymer solution. The prepolymer solution was brought to 37°C with a water bath and degassed at 0.1 bar for 15 minutes. After degassing, polymerization is initiated by adding 0.1% v/v tetramethylethylenediamine (TEMED) and 1% v/v APS solution to the monomers. The resulting solution was mixed and dispensed in silicone molds and a methacrylated glass coverslip was used to seal the mold. Once polymerized, the gels were detached from the molds and placed in milliQ water.

Glutathione (GSH) mediated softening

For all softening experiments, GSH was freshly dissolved in DMEM medium to a final 1-20mM concentration. For mechanical measurements during softening, the gels were pre-equilibrated at 37°C with complete culture medium (DMEM supplemented with 10%FBS and 1% P/S). Then, the medium was replaced with GSH supplemented medium at the required concentration. At the given timepoint, gels were rinsed with PBS and their elastic moduli were measured. For *in-situ* softening during cell

culture a 2X concentrated softening medium was used to dilute 1:1 the culture medium to obtain the final working concentration.

Micropipette aspiration measurements

For measurements of the bulk Young's modulus, hydrogel samples were prepared and swelled overnight in 1XPBS. The measurement setup, consisting of a glass capillary connected to a syringe pump and a pressure sensor, was mounted on an inverted optical microscope, with a sample holder perpendicular to the imaging plane. The gel-supporting glass coverslip was placed on the holder and the capillary was moved towards the surface of the gel until full contact was achieved.
Then, by aspiration of the syringe pump, a negative pressure was applied to the sample surface through the capillary and an image of the aspirated gel meniscus was taken simultaneously to a pressure reading with a sensor. The collected image was processed with a MatLab image analysis program to obtain the aspirated length of the gel inside the glass pipette, and the stiffness of the material was obtained using a model that correlates the aspirated length and exerted pressure with the Young's modulus. Details of the measurement setup are reported in reference [197].

AFM measurements

AFM measurements were conducted with the sample immersed in liquid. Elastic moduli were derived from the force-distance curves by fitting with a Hertz model considering a blunted pyramidal probe geometry.

Hydrogels mesh size measurements

The mesh size was estimated by observing the exclusion of fluorescent probes of known size in a 1XPBS solution. Hydrogel samples were placed in a glass bottom dish and swollen for 24h in 1XPBS. Then, the PBS used for swelling was replaced with a solution of fluorescent dextrans (or 100nm diameter FITC-labelled polystyrene nanospheres) and a confocal image of the gel-solution interface was collected. To allow for probe diffusion in the material, the gel was let in the solution for an additional 24h and after replacing the solution with fresh PBS, a second image was acquired to assess whether the fluorescent probes were excluded from the material. The mesh size was determined as the range of sizes between the largest diffusing probe and the smallest excluded one.
The following equations used to calculate the intrinsic viscosity $[\eta]$ and the hydro- dynamic radius Rh of the dextrans:

$$[\eta] = KM^{a}(\mathrm{mL\,g^{-1}})$$

$$R_h = \left(\frac{3\,[\eta]M}{10\pi N}\right)^{\frac{1}{3}}\ (\mathrm{cm})$$

where $[\eta]$ is expressed in (mL g^{-1}) and is empirically related to molecular weight by the Mark–Houwink equation (1) , and Rh is the hydrodynamic radius in Equation (2)[207]. The *K* and *a* parameters (K = 0.1361 mL g^{-1} and a = 0.45) for dextrans are polymer-specific and depend on the temperature and the kind of solvent, the values used are reported in the literature[208].

Immunofluorescence

Cells cultured on hydrogels were washed with PBS and fixed for 15 min in 4% PFA in PBS, then, samples were washed two times in PBS and permeabilized for 10 min with 0.3% Triton X-100. Samples were then washed three times in PBS and blocked with 10% goat serum for 1h.
The following incubations were performed with 2% goat serum in PBS-t (0.1% Triton X-100 in PBS) as a buffer. Primary antibodies were diluted in the buffer and incubations were performed overnight at 4°C in a humid chamber.
For F-actin labelling, samples were incubated 30' with AF568-phalloidin (1:100 dilution).
After 5 washes in PBS-t, secondary antibody incubation was performed with AlexaFluor coupled antibodies for 2h at room temperature in the dark. Following 5 washes in PBS-t, nuclei were stained by incubation with Hoechst 33342 (1:1000 dilution in incubation buffer) for 10' and mounted with prolong diamond (Invitrogen) mountant.

Antibodies
Integrin α5β1 novus NBP2-52680 (1:100)
Integrin αvβ3 chemicon LM609 (1:100)
YAP Santa Cruz Biotech sc-101199 (1:100)
Laminin Invitrogen PA1-16730 (1:200)
Paxillin BD 612405 (1:1000)

Microscopy

Confocal images were acquired on a Leica STELLARIS 5 microscope. For long-term time-lapse imaging the sample chamber was maintained at 37 °C and 5% CO_2.

Quantification of Nuclear/Cytosolic fluorescence intensity ratios

To quantify the ratio of nuclear to cytosol YAP/TAZ signal, confocal images of samples immunostained for YAP/TAZ were analyzed with CellProfiler pipeline. The process involved outlining the nuclear projected area, and a cell area mask based on the Hoechst and phalloidin signal respectively. The ratio N/C was then calculated by dividing the intensity in the nuclear area by the one in the cytosol (the latter obtained by subtracting the nucleus from the cell area).

REFERENCES

1 Iskratsch, T., Wolfenson, H. & Sheetz, M. P. Appreciating force and shape-the rise of mechanotransduction in cell biology. *Nat Rev Mol Cell Biol* **15**, 825-833 (2014). https://doi.org:10.1038/nrm3903

2 Chen, C. S., Mrksich, M., Huang, S., Whitesides, G. M. & Ingber, D. E. Geometric control of cell life and death. *Science* **276**, 1425-1428 (1997). https://doi.org:10.1126/science.276.5317.1425

3 Pelham, R. J., Jr. & Wang, Y. Cell locomotion and focal adhesions are regulated by substrate flexibility. *Proc Natl Acad Sci U S A* **94**, 13661-13665 (1997). https://doi.org:10.1073/pnas.94.25.13661

4 Engler, A. J., Sen, S., Sweeney, H. L. & Discher, D. E. Matrix elasticity directs stem cell lineage specification. *Cell* **126**, 677-689 (2006). https://doi.org:10.1016/j.cell.2006.06.044

5 Janmey, P. A., Fletcher, D. A. & Reinhart-King, C. A. Stiffness Sensing by Cells. *Physiol Rev* **100**, 695-724 (2020). https://doi.org:10.1152/physrev.00013.2019

6 Discher, D. E., Janmey, P. & Wang, Y. L. Tissue cells feel and respond to the stiffness of their substrate. *Science* **310**, 1139-1143 (2005). https://doi.org:10.1126/science.1116995

7 Lo, C. M., Wang, H. B., Dembo, M. & Wang, Y. L. Cell movement is guided by the rigidity of the substrate. *Biophys J* **79**, 144-152 (2000). https://doi.org:10.1016/S0006-3495(00)76279-5

8 Vogel, V. & Sheetz, M. Local force and geometry sensing regulate cell functions. *Nat Rev Mol Cell Biol* **7**, 265-275 (2006). https://doi.org:10.1038/nrm1890

9 Butcher, D. T., Alliston, T. & Weaver, V. M. A tense situation: forcing tumour progression. *Nat Rev Cancer* **9**, 108-122 (2009). https://doi.org:10.1038/nrc2544

10 Jaalouk, D. E. & Lammerding, J. Mechanotransduction gone awry. *Nat Rev Mol Cell Biol* **10**, 63-73 (2009). https://doi.org:10.1038/nrm2597

11 Shin, J. Y. & Worman, H. J. Molecular Pathology of Laminopathies. *Annu Rev Pathol* **17**, 159-180 (2022). https://doi.org:10.1146/annurev-pathol-042220-034240

12 Brusatin, G., Panciera, T., Gandin, A., Citron, A. & Piccolo, S. Biomaterials and engineered microenvironments to control YAP/TAZ-dependent cell behaviour. *Nat Mater* **17**, 1063-1075 (2018). https://doi.org:10.1038/s41563-018-0180-8

13 Hersel, U., Dahmen, C. & Kessler, H. RGD modified polymers: biomaterials for stimulated cell adhesion and beyond. *Biomaterials* **24**, 4385-4415 (2003). https://doi.org:10.1016/s0142-9612(03)00343-0

14 Alberts, B. *et al. Molecular Biology of the Cell*. (2017).

15 Humphrey, J. D., Dufresne, E. R. & Schwartz, M. A. Mechanotransduction and extracellular matrix homeostasis. *Nat Rev Mol Cell Biol* **15**, 802-812 (2014). https://doi.org:10.1038/nrm3896

16 Emsley, J., Knight, C. G., Farndale, R. W., Barnes, M. J. & Liddington, R. C. Structural basis of collagen recognition by integrin alpha2beta1. *Cell* **101**, 47-56 (2000). https://doi.org:10.1016/S0092-8674(00)80622-4

17 Davis, G. E. Affinity of integrins for damaged extracellular matrix: alpha v beta 3 binds to denatured collagen type I through RGD sites. *Biochem Biophys Res Commun* **182**, 1025-1031 (1992). https://doi.org:10.1016/0006-291x(92)91834-d

18 Iozzo, R. V. & Schaefer, L. Proteoglycan form and function: A comprehensive nomenclature of proteoglycans. *Matrix Biol* **42**, 11-55 (2015). https://doi.org:10.1016/j.matbio.2015.02.003

19 Roughley, P. J. & Mort, J. S. The role of aggrecan in normal and osteoarthritic cartilage. *J Exp Orthop* **1**, 8 (2014). https://doi.org:10.1186/s40634-014-0008-7

20 Klein, E. A. *et al.* Cell-cycle control by physiological matrix elasticity and in vivo tissue stiffening. *Curr Biol* **19**, 1511-1518 (2009). https://doi.org:10.1016/j.cub.2009.07.069

21 Egeblad, M., Rasch, M. G. & Weaver, V. M. Dynamic interplay between the collagen scaffold and tumor evolution. *Curr Opin Cell Biol* **22**, 697-706 (2010). https://doi.org:10.1016/j.ceb.2010.08.015

22 Daley, W. P., Peters, S. B. & Larsen, M. Extracellular matrix dynamics in development and regenerative medicine. *J Cell Sci* **121**, 255-264 (2008). https://doi.org:10.1242/jcs.006064

23 Piersma, B., Hayward, M. K. & Weaver, V. M. Fibrosis and cancer: A strained relationship. *Biochim Biophys Acta Rev Cancer* **1873**, 188356 (2020). https://doi.org:10.1016/j.bbcan.2020.188356

24 Sun, Z., Costell, M. & Fassler, R. Integrin activation by talin, kindlin and mechanical forces. *Nat Cell Biol* **21**, 25-31 (2019). https://doi.org:10.1038/s41556-018-0234-9

25 Kechagia, J. Z., Ivaska, J. & Roca-Cusachs, P. Integrins as biomechanical sensors of the microenvironment. *Nat Rev Mol Cell Biol* **20**, 457-473 (2019). https://doi.org:10.1038/s41580-019-0134-2

26 Seetharaman, S. & Etienne-Manneville, S. Integrin diversity brings specificity in mechanotransduction. *Biol Cell* **110**, 49-64 (2018). https://doi.org:10.1111/boc.201700060

27 Roca-Cusachs, P., Gauthier, N. C., Del Rio, A. & Sheetz, M. P. Clustering of alpha(5)beta(1) integrins determines adhesion strength whereas alpha(v)beta(3) and talin enable mechanotransduction. *Proc Natl Acad Sci U S A* **106**, 16245-16250 (2009). https://doi.org:10.1073/pnas.0902818106

28 Elosegui-Artola, A. *et al.* Rigidity sensing and adaptation through regulation of integrin types. *Nat Mater* **13**, 631-637 (2014). https://doi.org:10.1038/nmat3960

29 Schiller, H. B. *et al.* beta1- and alphav-class integrins cooperate to regulate myosin II during rigidity sensing of fibronectin-based microenvironments. *Nat Cell Biol* **15**, 625-636 (2013). https://doi.org:10.1038/ncb2747

30 Hakkinen, K. M., Harunaga, J. S., Doyle, A. D. & Yamada, K. M. Direct comparisons of the morphology, migration, cell adhesions, and actin cytoskeleton of fibroblasts in four different three-dimensional extracellular matrices. *Tissue Eng Part A* **17**, 713-724 (2011). https://doi.org:10.1089/ten.TEA.2010.0273

31 Riveline, D. *et al.* Focal contacts as mechanosensors: externally applied local mechanical force induces growth of focal contacts by an mDia1-dependent and ROCK-independent mechanism. *J Cell Biol* **153**, 1175-1186 (2001). https://doi.org:10.1083/jcb.153.6.1175

32 Galbraith, C. G., Yamada, K. M. & Sheetz, M. P. The relationship between force and focal complex development. *J Cell Biol* **159**, 695-705 (2002). https://doi.org:10.1083/jcb.200204153

33 Geiger, B., Bershadsky, A., Pankov, R. & Yamada, K. M. Transmembrane crosstalk between the extracellular matrix--cytoskeleton crosstalk. *Nat Rev Mol Cell Biol* **2**, 793-805 (2001). https://doi.org:10.1038/35099066

34 Pasapera, A. M., Schneider, I. C., Rericha, E., Schlaepfer, D. D. & Waterman, C. M. Myosin II activity regulates vinculin recruitment to focal adhesions through FAK-mediated paxillin phosphorylation. *J Cell Biol* **188**, 877-890 (2010). https://doi.org:10.1083/jcb.200906012

35 Zaidel-Bar, R., Ballestrem, C., Kam, Z. & Geiger, B. Early molecular events in the assembly of matrix adhesions at the leading edge of migrating cells. *J Cell Sci* **116**, 4605-4613 (2003). https://doi.org:10.1242/jcs.00792

36 Mitra, S. K., Hanson, D. A. & Schlaepfer, D. D. Focal adhesion kinase: in command and control of cell motility. *Nat Rev Mol Cell Biol* **6**, 56-68 (2005). https://doi.org:10.1038/nrm1549

37 Morgan, M. R., Humphries, M. J. & Bass, M. D. Synergistic control of cell adhesion by integrins and syndecans. *Nat Rev Mol Cell Biol* **8**, 957-969 (2007). https://doi.org:10.1038/nrm2289

38 Choi, C. K. *et al.* Actin and alpha-actinin orchestrate the assembly and maturation of nascent adhesions in a myosin II motor-independent manner. *Nat Cell Biol* **10**, 1039-1050 (2008). https://doi.org:10.1038/ncb1763

39 Changede, R., Xu, X., Margadant, F. & Sheetz, M. P. Nascent Integrin Adhesions Form on All Matrix Rigidities after Integrin Activation. *Dev Cell* **35**, 614-621 (2015). https://doi.org:10.1016/j.devcel.2015.11.001

40 Balaban, N. Q. *et al.* Force and focal adhesion assembly: a close relationship studied using elastic micropatterned substrates. *Nat Cell Biol* **3**, 466-472 (2001). https://doi.org:10.1038/35074532

41 Lavelin, I. *et al.* Differential effect of actomyosin relaxation on the dynamic properties of focal adhesion proteins. *Plos One* **8**, e73549 (2013). https://doi.org:10.1371/journal.pone.0073549

42 Quirk, R. A., Chan, W. C., Davies, M. C., Tendler, S. J. & Shakesheff, K. M. Poly(L-lysine)-GRGDS as a biomimetic surface modifier for poly(lactic acid). *Biomaterials* **22**, 865-872 (2001). https://doi.org:10.1016/s0142-9612(00)00250-7

43 Grashoff, C. *et al.* Measuring mechanical tension across vinculin reveals regulation of focal adhesion dynamics. *Nature* **466**, 263-266 (2010). https://doi.org:10.1038/nature09198

44 Bershadsky, A., Chausovsky, A., Becker, E., Lyubimova, A. & Geiger, B. Involvement of microtubules in the control of adhesion-dependent signal transduction. *Curr Biol* **6**, 1279-1289 (1996). https://doi.org:10.1016/s0960-9822(02)70714-8

45 Schiller, H. B., Friedel, C. C., Boulegue, C. & Fassler, R. Quantitative proteomics of the integrin adhesome show a myosin II-dependent recruitment of LIM domain proteins. *EMBO Rep* **12**, 259-266 (2011). https://doi.org:10.1038/embor.2011.5

46 Mori, Y., Akedo, H. & Tanigaki, Y. Changes induced by concanavalin A in morphological and adhesive properties of suspension cells. *Exp Cell Res* **78**, 360-366 (1973). https://doi.org:10.1016/0014-4827(73)90080-3

47 Mazia, D., Schatten, G. & Sale, W. Adhesion of cells to surfaces coated with polylysine. Applications to electron microscopy. *J Cell Biol* **66**, 198-200 (1975). https://doi.org:10.1083/jcb.66.1.198

48 Ezratty, E. J., Partridge, M. A. & Gundersen, G. G. Microtubule-induced focal adhesion disassembly is mediated by dynamin and focal adhesion kinase. *Nat Cell Biol* **7**, 581-590 (2005). https://doi.org:10.1038/ncb1262

49 Krylyshkina, O. *et al.* Modulation of substrate adhesion dynamics via microtubule targeting requires kinesin-1. *J Cell Biol* **156**, 349-359 (2002). https://doi.org:10.1083/jcb.200105051

50 Bhatt, A., Kaverina, I., Otey, C. & Huttenlocher, A. Regulation of focal complex composition and disassembly by the calcium-dependent protease calpain. *J Cell Sci* **115**, 3415-3425 (2002). https://doi.org:10.1242/jcs.115.17.3415

51 Yamada, K. M. & Sixt, M. Mechanisms of 3D cell migration. *Nat Rev Mol Cell Biol* **20**, 738-752 (2019). https://doi.org:10.1038/s41580-019-0172-9

52 Ingber, D. E., Wang, N. & Stamenovic, D. Tensegrity, cellular biophysics, and the mechanics of living systems. *Rep Prog Phys* **77**, 046603 (2014). https://doi.org:10.1088/0034-4885/77/4/046603

53 Pellegrin, S. & Mellor, H. Actin stress fibres. *J Cell Sci* **120**, 3491-3499 (2007). https://doi.org:10.1242/jcs.018473

54 Hotulainen, P. & Lappalainen, P. Stress fibers are generated by two distinct actin assembly mechanisms in motile cells. *J Cell Biol* **173**, 383-394 (2006). https://doi.org:10.1083/jcb.200511093

55 Maninova, M. & Vomastek, T. Dorsal stress fibers, transverse actin arcs, and perinuclear actin fibers form an interconnected network that induces nuclear movement in polarizing fibroblasts. *FEBS J* **283**, 3676-3693 (2016). https://doi.org:10.1111/febs.13836

56 Webb, D. J., Parsons, J. T. & Horwitz, A. F. Adhesion assembly, disassembly and turnover in migrating cells -- over and over and over again. *Nat Cell Biol* **4**, E97-100 (2002). https://doi.org:10.1038/ncb0402-e97

57 Wu, C. *et al.* Arp2/3 is critical for lamellipodia and response to extracellular matrix cues but is dispensable for chemotaxis. *Cell* **148**, 973-987 (2012). https://doi.org:10.1016/j.cell.2011.12.034

58 Doss, B. L. *et al.* Cell response to substrate rigidity is regulated by active and passive cytoskeletal stress. *Proc Natl Acad Sci U S A* **117**, 12817-12825 (2020). https://doi.org:10.1073/pnas.1917555117

59 Smith, M. A. *et al.* A zyxin-mediated mechanism for actin stress fiber maintenance and repair. *Dev Cell* **19**, 365-376 (2010). https://doi.org:10.1016/j.devcel.2010.08.008

60 Wang, D. *et al.* A stretching device for imaging real-time molecular dynamics of live cells adhering to elastic membranes on inverted microscopes during the entire process of the stretch. *Integr Biol (Camb)* **2**, 288-293 (2010). https://doi.org:10.1039/b920644b

61 Prager-Khoutorsky, M. *et al.* Fibroblast polarization is a matrix-rigidity-dependent process controlled by focal adhesion mechanosensing. *Nat Cell Biol* **13**, 1457-1465 (2011). https://doi.org:10.1038/ncb2370

62 Andreu, I. *et al.* The force loading rate drives cell mechanosensing through both reinforcement and cytoskeletal softening. *Nat Commun* **12**, 4229 (2021). https://doi.org:10.1038/s41467-021-24383-3

63 Small, J. V., Geiger, B., Kaverina, I. & Bershadsky, A. How do microtubules guide migrating cells? *Nat Rev Mol Cell Biol* **3**, 957-964 (2002). https://doi.org:10.1038/nrm971

64 Ingber, D. E. Tensegrity I. Cell structure and hierarchical systems biology. *J Cell Sci* **116**, 1157-1173 (2003). https://doi.org:10.1242/jcs.00359

65 Small, J. V. & Kaverina, I. Microtubules meet substrate adhesions to arrange cell polarity. *Curr Opin Cell Biol* **15**, 40-47 (2003). https://doi.org:10.1016/s0955-0674(02)00008-x

66 Piccolo, S., Dupont, S. & Cordenonsi, M. The biology of YAP/TAZ: hippo signaling and beyond. *Physiol Rev* **94**, 1287-1312 (2014). https://doi.org:10.1152/physrev.00005.2014

67 Totaro, A., Panciera, T. & Piccolo, S. YAP/TAZ upstream signals and downstream responses. *Nat Cell Biol* **20**, 888-899 (2018). https://doi.org:10.1038/s41556-018-0142-z

68 Halder, G., Dupont, S. & Piccolo, S. Transduction of mechanical and cytoskeletal cues by YAP and TAZ. *Nat Rev Mol Cell Biol* **13**, 591-600 (2012). https://doi.org:10.1038/nrm3416

69 Dupont, S. *et al.* Role of YAP/TAZ in mechanotransduction. *Nature* **474**, 179-183 (2011). https://doi.org:10.1038/nature10137

70 Aragona, M. *et al.* A mechanical checkpoint controls multicellular growth through YAP/TAZ regulation by actin-processing factors. *Cell* **154**, 1047-1059 (2013). https://doi.org:10.1016/j.cell.2013.07.042

71 Ondeck, M. G. *et al.* Dynamically stiffened matrix promotes malignant transformation of mammary epithelial cells via collective mechanical signaling. *Proc Natl Acad Sci U S A* **116**, 3502-3507 (2019). https://doi.org:10.1073/pnas.1814204116

72 Yang, C., Tibbitt, M. W., Basta, L. & Anseth, K. S. Mechanical memory and dosing influence stem cell fate. *Nature Materials* **13**, 645-652 (2014). https://doi.org:10.1038/Nmat3889

73 Mannaerts, I. *et al.* The Hippo pathway effector YAP controls mouse hepatic stellate cell activation. *J Hepatol* **63**, 679-688 (2015). https://doi.org:10.1016/j.jhep.2015.04.011

74 Liu, F. *et al.* Mechanosignaling through YAP and TAZ drives fibroblast activation and fibrosis. *Am J Physiol Lung Cell Mol Physiol* **308**, L344-357 (2015). https://doi.org:10.1152/ajplung.00300.2014

75 Szeto, S. G. *et al.* YAP/TAZ Are Mechanoregulators of TGF-beta-Smad Signaling and Renal Fibrogenesis. *J Am Soc Nephrol* **27**, 3117-3128 (2016). https://doi.org:10.1681/ASN.2015050499

76 Kirby, T. J. & Lammerding, J. Emerging views of the nucleus as a cellular mechanosensor. *Nat Cell Biol* **20**, 373-381 (2018). https://doi.org:10.1038/s41556-018-0038-y

77 Lomakin, A. J. *et al.* The nucleus acts as a ruler tailoring cell responses to spatial constraints. *Science* **370** (2020). https://doi.org:10.1126/science.aba2894

78 Pajerowski, J. D., Dahl, K. N., Zhong, F. L., Sammak, P. J. & Discher, D. E. Physical plasticity of the nucleus in stem cell differentiation. *Proc Natl Acad Sci U S A* **104**, 15619-15624 (2007). https://doi.org:10.1073/pnas.0702576104

79 Swift, J. *et al.* Nuclear lamin-A scales with tissue stiffness and enhances matrix-directed differentiation. *Science* **341**, 1240104 (2013). https://doi.org:10.1126/science.1240104

80 Elosegui-Artola, A. *et al.* Force Triggers YAP Nuclear Entry by Regulating Transport across Nuclear Pores. *Cell* **171**, 1397-1410 e1314 (2017). https://doi.org:10.1016/j.cell.2017.10.008

81 Denais, C. M. *et al.* Nuclear envelope rupture and repair during cancer cell migration. *Science* **352**, 353-358 (2016). https://doi.org:10.1126/science.aad7297

82 Thiam, H. R. *et al.* Perinuclear Arp2/3-driven actin polymerization enables nuclear deformation to facilitate cell migration through complex environments. *Nat Commun* **7**, 10997 (2016). https://doi.org:10.1038/ncomms10997

83 Khatau, S. B. *et al.* A perinuclear actin cap regulates nuclear shape. *P Natl Acad Sci USA* **106**, 19017-19022 (2009). https://doi.org:10.1073/pnas.0908686106

84 Kim, D. H. *et al.* Actin cap associated focal adhesions and their distinct role in cellular mechanosensing. *Sci Rep-Uk* **2** (2012). https://doi.org:ARTN 555
10.1038/srep00555

85 Shiu, J. Y., Aires, L., Lin, Z. & Vogel, V. Nanopillar force measurements reveal actin-cap-mediated YAP mechanotransduction. *Nat Cell Biol* **20**, 262-271 (2018). https://doi.org:10.1038/s41556-017-0030-y

86 Reinhart-King, C. A., Dembo, M. & Hammer, D. A. Cell-cell mechanical communication through compliant substrates. *Biophys J* **95**, 6044-6051 (2008). https://doi.org:10.1529/biophysj.107.127662

87 Parsons, J. T., Horwitz, A. R. & Schwartz, M. A. Cell adhesion: integrating cytoskeletal dynamics and cellular tension. *Nat Rev Mol Cell Biol* **11**, 633-643 (2010). https://doi.org:10.1038/nrm2957

88 Yao, M. *et al.* The mechanical response of talin. *Nat Commun* **7**, 11966 (2016). https://doi.org:10.1038/ncomms11966

89 Elosegui-Artola, A. *et al.* Mechanical regulation of a molecular clutch defines force transmission and transduction in response to matrix rigidity. *Nat Cell Biol* **18**, 540-548 (2016). https://doi.org:10.1038/ncb3336

90 Schwarz, U. S. & Gardel, M. L. United we stand: integrating the actin cytoskeleton and cell-matrix adhesions in cellular mechanotransduction. *J Cell Sci* **125**, 3051-3060 (2012). https://doi.org:10.1242/jcs.093716

91 Johnson, H. E. *et al.* F-actin bundles direct the initiation and orientation of lamellipodia through adhesion-based signaling. *J Cell Biol* **208**, 443-455 (2015). https://doi.org:10.1083/jcb.201406102

92 Wong, S., Guo, W. H. & Wang, Y. L. Fibroblasts probe substrate rigidity with filopodia extensions before occupying an area. *Proc Natl Acad Sci U S A* **111**, 17176-17181 (2014). https://doi.org:10.1073/pnas.1412285111

93 Wolfenson, H. *et al.* Tropomyosin controls sarcomere-like contractions for rigidity sensing and suppressing growth on soft matrices. *Nat Cell Biol* **18**, 33-42 (2016). https://doi.org:10.1038/ncb3277

94 Yeung, T. *et al.* Effects of substrate stiffness on cell morphology, cytoskeletal structure, and adhesion. *Cell Motil Cytoskeleton* **60**, 24-34 (2005). https://doi.org:10.1002/cm.20041

95 Yang, B. *et al.* Stopping transformed cancer cell growth by rigidity sensing. *Nat Mater* **19**, 239-250 (2020). https://doi.org:10.1038/s41563-019-0507-0

96 Stanton, A. E., Tong, X. & Yang, F. Extracellular matrix type modulates mechanotransduction of stem cells. *Acta Biomater* **96**, 310-320 (2019). https://doi.org:10.1016/j.actbio.2019.06.048

97 Oria, R. *et al.* Force loading explains spatial sensing of ligands by cells. *Nature* **552**, 219-224 (2017). https://doi.org:10.1038/nature24662

98 Mih, J. D., Marinkovic, A., Liu, F., Sharif, A. S. & Tschumperlin, D. J. Matrix stiffness reverses the effect of actomyosin tension on cell proliferation. *J Cell Sci* **125**, 5974-5983 (2012). https://doi.org:10.1242/jcs.108886

99 Chowdhury, F. *et al.* Material properties of the cell dictate stress-induced spreading and differentiation in embryonic stem cells. *Nat Mater* **9**, 82-88 (2010). https://doi.org:10.1038/nmat2563

100 Panzetta, V., Fusco, S. & Netti, P. A. Cell mechanosensing is regulated by substrate strain energy rather than stiffness. *Proc Natl Acad Sci U S A* **116**, 22004-22013 (2019). https://doi.org:10.1073/pnas.1904660116

101 Elosegui-Artola, A., Trepat, X. & Roca-Cusachs, P. Control of Mechanotransduction by Molecular Clutch Dynamics. *Trends Cell Biol* **28**, 356-367 (2018). https://doi.org:10.1016/j.tcb.2018.01.008

102 Schultz, G. S., Davidson, J. M., Kirsner, R. S., Bornstein, P. & Herman, I. M. Dynamic reciprocity in the wound microenvironment. *Wound Repair Regen* **19**, 134-148 (2011). https://doi.org:10.1111/j.1524-475X.2011.00673.x

103 Na, S. *et al.* Rapid signal transduction in living cells is a unique feature of mechanotransduction. *Proc Natl Acad Sci U S A* **105**, 6626-6631 (2008). https://doi.org:10.1073/pnas.0711704105

104 Maniotis, A. J., Chen, C. S. & Ingber, D. E. Demonstration of mechanical connections between integrins, cytoskeletal filaments, and nucleoplasm that stabilize nuclear structure. *Proc Natl Acad Sci U S A* **94**, 849-854 (1997). https://doi.org:10.1073/pnas.94.3.849

105 Strohmeyer, N., Bharadwaj, M., Costell, M., Fassler, R. & Muller, D. J. Fibronectin-bound alpha5beta1 integrins sense load and signal to reinforce adhesion in less than a second. *Nat Mater* **16**, 1262-1270 (2017). https://doi.org:10.1038/nmat5023

106 Wolfenson, H., Yang, B. & Sheetz, M. P. Steps in Mechanotransduction Pathways that Control Cell Morphology. *Annu Rev Physiol* **81**, 585-605 (2019). https://doi.org:10.1146/annurev-physiol-021317-121245

107 Dembo, M. & Wang, Y. L. Stresses at the cell-to-substrate interface during locomotion of fibroblasts. *Biophys J* **76**, 2307-2316 (1999). https://doi.org:10.1016/S0006-3495(99)77386-8

108 Saldin, L. T., Cramer, M. C., Velankar, S. S., White, L. J. & Badylak, S. F. Extracellular matrix hydrogels from decellularized tissues: Structure and function. *Acta Biomater* **49**, 1-15 (2017). https://doi.org:10.1016/j.actbio.2016.11.068

109 Antoine, E. E., Vlachos, P. P. & Rylander, M. N. Tunable collagen I hydrogels for engineered physiological tissue micro-environments. *Plos One* **10**, e0122500 (2015). https://doi.org:10.1371/journal.pone.0122500

110 Caliari, S. R. & Burdick, J. A. A practical guide to hydrogels for cell culture. *Nat Methods* **13**, 405-414 (2016). https://doi.org:10.1038/nmeth.3839

111 Harris, A. K., Wild, P. & Stopak, D. Silicone rubber substrata: a new wrinkle in the study of cell locomotion. *Science* **208**, 177-179 (1980). https://doi.org:10.1126/science.6987736

112 Gelfi, C. & Righetti, P. G. Polymerization kinetics of polyacrylamide gels I. Effect of different cross-linkers. *Electrophoresis* **2**, 213-219 (1981). https://doi.org:10.1002/elps.1150020404

113 Zhang, B. *et al.* Highly stretchable hydrogels for UV curing based high-resolution multimaterial 3D printing. *J Mater Chem B* **6**, 3246-3253 (2018). https://doi.org:10.1039/c8tb00673c

114 Beningo, K. A., Dembo, M. & Wang, Y. L. Responses of fibroblasts to anchorage of dorsal extracellular matrix receptors. *Proc Natl Acad Sci U S A* **101**, 18024-18029 (2004). https://doi.org:10.1073/pnas.0405747102

115 Oyen, M. L. Mechanical characterisation of hydrogel materials. *International Materials Reviews* **59**, 44-59 (2013). https://doi.org:10.1179/1743280413y.0000000022

116 Denisin, A. K. & Pruitt, B. L. Tuning the Range of Polyacrylamide Gel Stiffness for Mechanobiology Applications. *ACS Appl Mater Interfaces* **8**, 21893-21902 (2016). https://doi.org:10.1021/acsami.5b09344

117 Tse, J. R. & Engler, A. J. Preparation of hydrogel substrates with tunable mechanical properties. *Curr Protoc Cell Biol* **Chapter 10**, Unit 10 16 (2010). https://doi.org:10.1002/0471143030.cb1016s47

118 Lee, S., Stanton, A. E., Tong, X. & Yang, F. Hydrogels with enhanced protein conjugation efficiency reveal stiffness-induced YAP localization in stem cells depends on biochemical cues. *Biomaterials* **202**, 26-34 (2019). https://doi.org:10.1016/j.biomaterials.2019.02.021

119 Lee, J. P., Kassianidou, E., MacDonald, J. I., Francis, M. B. & Kumar, S. N-terminal specific conjugation of extracellular matrix proteins to 2-pyridinecarboxaldehyde functionalized polyacrylamide hydrogels. *Biomaterials* **102**, 268-276 (2016). https://doi.org:10.1016/j.biomaterials.2016.06.022

120 Isenberg, B. C., Dimilla, P. A., Walker, M., Kim, S. & Wong, J. Y. Vascular smooth muscle cell durotaxis depends on substrate stiffness gradient strength. *Biophys J* **97**, 1313-1322 (2009). https://doi.org:10.1016/j.bpj.2009.06.021

121 Tse, J. R. & Engler, A. J. Stiffness gradients mimicking in vivo tissue variation regulate mesenchymal stem cell fate. *Plos One* **6**, e15978 (2011). https://doi.org:10.1371/journal.pone.0015978

122 Wong, J. Y., Velasco, A., Rajagopalan, P. & Pham, Q. Directed Movement of Vascular Smooth Muscle Cells on Gradient-Compliant Hydrogels. *Langmuir* **19**, 1908-1913 (2003). https://doi.org:10.1021/la026403p

123 Ng, M. R., Besser, A., Danuser, G. & Brugge, J. S. Substrate stiffness regulates cadherin-dependent collective migration through myosin-II contractility. *J Cell Biol* **199**, 545-563 (2012). https://doi.org:10.1083/jcb.201207148

124 Fairbanks, B. D., Schwartz, M. P., Bowman, C. N. & Anseth, K. S. Photoinitiated polymerization of PEG-diacrylate with lithium phenyl-2,4,6-trimethylbenzoylphosphinate: polymerization rate and cytocompatibility. *Biomaterials* **30**, 6702-6707 (2009). https://doi.org:10.1016/j.biomaterials.2009.08.055

125 Salinas, C. N. & Anseth, K. S. Mixed Mode Thiol−Acrylate Photopolymerizations for the Synthesis of PEG−Peptide Hydrogels. *Macromolecules* **41**, 6019-6026 (2008). https://doi.org:10.1021/ma800621h

126 Lutolf, M. P. & Hubbell, J. A. Synthesis and physicochemical characterization of end-linked poly(ethylene glycol)-co-peptide hydrogels formed by Michael-type addition. *Biomacromolecules* **4**, 713-722 (2003). https://doi.org:10.1021/bm025744e

127 Lutolf, M. P. *et al.* Repair of bone defects using synthetic mimetics of collagenous extracellular matrices. *Nat Biotechnol* **21**, 513-518 (2003). https://doi.org:10.1038/nbt818

128 Williams, C. G., Malik, A. N., Kim, T. K., Manson, P. N. & Elisseeff, J. H. Variable cytocompatibility of six cell lines with photoinitiators used for polymerizing hydrogels and cell encapsulation. *Biomaterials* **26**, 1211-1218 (2005). https://doi.org:10.1016/j.biomaterials.2004.04.024

129 Hern, D. L. & Hubbell, J. A. Incorporation of adhesion peptides into nonadhesive hydrogels useful for tissue resurfacing. *Journal of Biomedical Materials Research* **39**, 266-276 (1998). https://doi.org:10.1002/(sici)1097-4636(199802)39:2<266::Aid-jbm14>3.0.Co;2-b

130 Laurent, T. C., Laurent, U. B. & Fraser, J. R. Functions of hyaluronan. *Ann Rheum Dis* **54**, 429-432 (1995). https://doi.org:10.1136/ard.54.5.429

131 Girish, K. S. & Kemparaju, K. The magic glue hyaluronan and its eraser hyaluronidase: a biological overview. *Life Sci* **80**, 1921-1943 (2007). https://doi.org:10.1016/j.lfs.2007.02.037

132 Burdick, J. A. & Prestwich, G. D. Hyaluronic acid hydrogels for biomedical applications. *Adv Mater* **23**, H41-56 (2011). https://doi.org:10.1002/adma.201003963

133 Burdick, J. A., Chung, C., Jia, X., Randolph, M. A. & Langer, R. Controlled degradation and mechanical behavior of photopolymerized hyaluronic acid networks. *Biomacromolecules* **6**, 386-391 (2005). https://doi.org:10.1021/bm049508a

134 Baier Leach, J., Bivens, K. A., Patrick, C. W., Jr. & Schmidt, C. E. Photocrosslinked hyaluronic acid hydrogels: natural, biodegradable tissue engineering scaffolds. *Biotechnol Bioeng* **82**, 578-589 (2003). https://doi.org:10.1002/bit.10605

135 Park, Y. D., Tirelli, N. & Hubbell, J. A. Photopolymerized hyaluronic acid-based hydrogels and interpenetrating networks. *Biomaterials* **24**, 893-900 (2003). https://doi.org:10.1016/s0142-9612(02)00420-9

136 Prestwich, G. D., Marecak, D. M., Marecek, J. F., Vercruysse, K. P. & Ziebell, M. R. Controlled chemical modification of hyaluronic acid: synthesis, applications, and biodegradation of hydrazide derivatives. *J Control Release* **53**, 93-103 (1998). https://doi.org:10.1016/s0168-3659(97)00242-3

137 Shu, X. Z., Liu, Y., Luo, Y., Roberts, M. C. & Prestwich, G. D. Disulfide cross-linked hyaluronan hydrogels. *Biomacromolecules* **3**, 1304-1311 (2002). https://doi.org:10.1021/bm025603c

138 Zheng Shu, X., Liu, Y., Palumbo, F. S., Luo, Y. & Prestwich, G. D. In situ crosslinkable hyaluronan hydrogels for tissue engineering. *Biomaterials* **25**, 1339-1348 (2004). https://doi.org:10.1016/j.biomaterials.2003.08.014

139 Shu, X. Z. *et al.* Attachment and spreading of fibroblasts on an RGD peptide-modified injectable hyaluronan hydrogel. *J Biomed Mater Res A* **68**, 365-375 (2004). https://doi.org:10.1002/jbm.a.20002

140 Ghosh, K. *et al.* Cell adaptation to a physiologically relevant ECM mimic with different viscoelastic properties. *Biomaterials* **28**, 671-679 (2007). https://doi.org:10.1016/j.biomaterials.2006.09.038

141 Cosgrove, B. D. *et al.* N-cadherin adhesive interactions modulate matrix mechanosensing and fate commitment of mesenchymal stem cells. *Nat Mater* **15**, 1297-1306 (2016). https://doi.org:10.1038/nmat4725

142 Ananthanarayanan, B., Kim, Y. & Kumar, S. Elucidating the mechanobiology of malignant brain tumors using a brain matrix-mimetic hyaluronic acid hydrogel platform. *Biomaterials* **32**, 7913-7923 (2011). https://doi.org:10.1016/j.biomaterials.2011.07.005

143 Knudson, W., Chow, G. & Knudson, C. B. CD44-mediated uptake and degradation of hyaluronan. *Matrix Biol* **21**, 15-23 (2002). https://doi.org:10.1016/s0945-053x(01)00186-x

144 Menzel, E. J. & Farr, C. Hyaluronidase and its substrate hyaluronan: biochemistry, biological activities and therapeutic uses. *Cancer Lett* **131**, 3-11 (1998). https://doi.org:10.1016/s0304-3835(98)00195-5

145 Harada, H. & Takahashi, M. CD44-dependent intracellular and extracellular catabolism of hyaluronic acid by hyaluronidase-1 and -2. *J Biol Chem* **282**, 5597-5607 (2007). https://doi.org:10.1074/jbc.M608358200

146 Chopra, A. *et al.* Augmentation of integrin-mediated mechanotransduction by hyaluronic acid. *Biomaterials* **35**, 71-82 (2014). https://doi.org:10.1016/j.biomaterials.2013.09.066

147 Chung, C. & Burdick, J. A. Influence of three-dimensional hyaluronic acid microenvironments on mesenchymal stem cell chondrogenesis. *Tissue Eng Part A* **15**, 243-254 (2009). https://doi.org:10.1089/ten.tea.2008.0067

148 Cohen, M., Kam, Z., Addadi, L. & Geiger, B. Dynamic study of the transition from hyaluronan- to integrin-mediated adhesion in chondrocytes. *EMBO J* **25**, 302-311 (2006). https://doi.org:10.1038/sj.emboj.7600960

149 Kim, Y. & Kumar, S. CD44-mediated adhesion to hyaluronic acid contributes to mechanosensing and invasive motility. *Mol Cancer Res* **12**, 1416-1429 (2014). https://doi.org:10.1158/1541-7786.MCR-13-0629

150 Pogoda, K. *et al.* Soft Substrates Containing Hyaluronan Mimic the Effects of Increased Stiffness on Morphology, Motility, and Proliferation of Glioma Cells. *Biomacromolecules* **18**, 3040-3051 (2017). https://doi.org:10.1021/acs.biomac.7b00324

151 Pritchard, R. H. & Terentjev, E. M. Swelling and de-swelling of gels under external elastic deformation. *Polymer* **54**, 6954-6960 (2013). https://doi.org:10.1016/j.polymer.2013.11.006

152 Doyle, A. D., Carvajal, N., Jin, A., Matsumoto, K. & Yamada, K. M. Local 3D matrix microenvironment regulates cell migration through spatiotemporal dynamics of contractility-dependent adhesions. *Nat Commun* **6**, 8720 (2015). https://doi.org:10.1038/ncomms9720

153 Buxboim, A., Rajagopal, K., Brown, A. E. & Discher, D. E. How deeply cells feel: methods for thin gels. *J Phys Condens Matter* **22**, 194116 (2010). https://doi.org:10.1088/0953-8984/22/19/194116

154 Lin, Y. C. *et al.* Mechanosensing of substrate thickness. *Phys Rev E Stat Nonlin Soft Matter Phys* **82**, 041918 (2010). https://doi.org:10.1103/PhysRevE.82.041918

155 Krieg, M. *et al.* Atomic force microscopy-based mechanobiology. *Nature Reviews Physics* **1**, 41-57 (2018). https://doi.org:10.1038/s42254-018-0001-7

156 Oyen, M. L. Nanoindentation of Biological and Biomimetic Materials. *Experimental Techniques* **37**, 73-87 (2013). https://doi.org:10.1111/j.1747-1567.2011.00716.x

157 Cameron, A. R., Frith, J. E. & Cooper-White, J. J. The influence of substrate creep on mesenchymal stem cell behaviour and phenotype. *Biomaterials* **32**, 5979-5993 (2011). https://doi.org:10.1016/j.biomaterials.2011.04.003

158 Chaudhuri, O. *et al.* Substrate stress relaxation regulates cell spreading. *Nat Commun* **6**, 6364 (2015). https://doi.org:10.1038/ncomms7365

159 Brown, M. A. *et al.* The use of mild trypsinization conditions in the detachment of endothelial cells to promote subsequent endothelialization on synthetic surfaces. *Biomaterials* **28**, 3928-3935 (2007). https://doi.org:10.1016/j.biomaterials.2007.05.009

160 Nasrollahi, S. *et al.* Past matrix stiffness primes epithelial cells and regulates their future collective migration through a mechanical memory. *Biomaterials* **146**, 146-155 (2017). https://doi.org:10.1016/j.biomaterials.2017.09.012

161 Kloxin, A. M., Kasko, A. M., Salinas, C. N. & Anseth, K. S. Photodegradable hydrogels for dynamic tuning of physical and chemical properties. *Science* **324**, 59-63 (2009). https://doi.org:10.1126/science.1169494

162 Frey, M. T. & Wang, Y. L. A photo-modulatable material for probing cellular responses to substrate rigidity. *Soft Matter* **5**, 1918-1924 (2009). https://doi.org:10.1039/b818104g

163 Norris, S. C. P., Soto, J., Kasko, A. M. & Li, S. Photodegradable Polyacrylamide Gels for Dynamic Control of Cell Functions. *ACS Appl Mater Interfaces* **13**, 5929-5944 (2021). https://doi.org:10.1021/acsami.0c19627

164 Tibbitt, M. W., Kloxin, A. M., Dyamenahalli, K. U. & Anseth, K. S. Controlled two-photon photodegradation of PEG hydrogels to study and manipulate subcellular interactions on soft materials. *Soft Matter* **6**, 5100-5108 (2010). https://doi.org:10.1039/C0SM00174K

165 Wang, H., Haeger, S. M., Kloxin, A. M., Leinwand, L. A. & Anseth, K. S. Redirecting Valvular Myofibroblasts into Dormant Fibroblasts through Light-mediated Reduction in Substrate Modulus. *Plos One* **7** (2012). https://doi.org:ARTN e39969
10.1371/journal.pone.0039969

166 Brown, T. E., Marozas, I. A. & Anseth, K. S. Amplified Photodegradation of Cell-Laden Hydrogels via an Addition-Fragmentation Chain Transfer Reaction. *Adv Mater* **29** (2017). https://doi.org:10.1002/adma.201605001

167 Killaars, A. R. *et al.* Extended Exposure to Stiff Microenvironments Leads to Persistent Chromatin Remodeling in Human Mesenchymal Stem Cells. *Adv Sci* **6** (2019). https://doi.org:ARTN 1801483
10.1002/advs.201801483

168 Guvendiren, M. & Burdick, J. A. Stiffening hydrogels to probe short- and long-term cellular responses to dynamic mechanics. *Nat Commun* **3**, 792 (2012). https://doi.org:10.1038/ncomms1792

169 Silver, J. S. *et al.* Injury-mediated stiffening persistently activates muscle stem cells through YAP and TAZ mechanotransduction. *Sci Adv* **7** (2021). https://doi.org:10.1126/sciadv.abe4501

170 Gunay, K. A. *et al.* PEG-Anthracene Hydrogels as an On-Demand Stiffening Matrix To Study Mechanobiology. *Angew Chem Int Ed Engl* **58**, 9912-9916 (2019). https://doi.org:10.1002/anie.201901989

171 Mabry, K. M., Lawrence, R. L. & Anseth, K. S. Dynamic stiffening of poly(ethylene glycol)-based hydrogels to direct valvular interstitial cell phenotype in a three-dimensional environment. *Biomaterials* **49**, 47-56 (2015). https://doi.org:10.1016/j.biomaterials.2015.01.047

172 Rosales, A. M., Vega, S. L., DelRio, F. W., Burdick, J. A. & Anseth, K. S. Hydrogels with Reversible Mechanics to Probe Dynamic Cell Microenvironments. *Angew Chem Int Edit* **56**, 12132-12136 (2017). https://doi.org:10.1002/anie.201705684

173 Rosales, A. M., Mabry, K. M., Nehls, E. M. & Anseth, K. S. Photoresponsive elastic properties of azobenzene-containing poly(ethylene-glycol)-based hydrogels. *Biomacromolecules* **16**, 798-806 (2015). https://doi.org:10.1021/bm501710e

174 Lee, I. N. *et al.* Photoresponsive Hydrogels with Photoswitchable Mechanical Properties Allow Time-Resolved Analysis of Cellular Responses to Matrix Stiffening. *ACS Appl Mater Interfaces* **10**, 7765-7776 (2018). https://doi.org:10.1021/acsami.7b18302

175 Horner, M. *et al.* Phytochrome-Based Extracellular Matrix with Reversibly Tunable Mechanical Properties. *Adv Mater* **31**, e1806727 (2019). https://doi.org:10.1002/adma.201806727

176 Zhu, J. Bioactive modification of poly(ethylene glycol) hydrogels for tissue engineering. *Biomaterials* **31**, 4639-4656 (2010). https://doi.org:10.1016/j.biomaterials.2010.02.044

177 Mahoney, M. J. & Anseth, K. S. Three-dimensional growth and function of neural tissue in degradable polyethylene glycol hydrogels. *Biomaterials* **27**, 2265-2274 (2006). https://doi.org:10.1016/j.biomaterials.2005.11.007

178 Zustiak, S. P. & Leach, J. B. Hydrolytically degradable poly(ethylene glycol) hydrogel scaffolds with tunable degradation and mechanical properties. *Biomacromolecules* **11**, 1348-1357 (2010). https://doi.org:10.1021/bm100137q

179 Hudalla, G. A., Eng, T. S. & Murphy, W. L. An approach to modulate degradation and mesenchymal stem cell behavior in poly(ethylene glycol) networks. *Biomacromolecules* **9**, 842-849 (2008). https://doi.org:10.1021/bm701179s

180 Caliari, S. R. *et al.* Gradually softening hydrogels for modeling hepatic stellate cell behavior during fibrosis regression. *Integr Biol-Uk* **8**, 720-728 (2016). https://doi.org:10.1039/c6ib00027d

181 Mann, B. K., Gobin, A. S., Tsai, A. T., Schmedlen, R. H. & West, J. L. Smooth muscle cell growth in photopolymerized hydrogels with cell adhesive and proteolytically degradable domains: synthetic ECM analogs for tissue engineering. *Biomaterials* **22**, 3045-3051 (2001). https://doi.org:10.1016/s0142-9612(01)00051-5

182 Cruz-Acuna, R. *et al.* Synthetic hydrogels for human intestinal organoid generation and colonic wound repair. *Nat Cell Biol* **19**, 1326-1335 (2017). https://doi.org:10.1038/ncb3632

183 Gjorevski, N. *et al.* Designer matrices for intestinal stem cell and organoid culture. *Nature* **539**, 560-564 (2016). https://doi.org:10.1038/nature20168

184 Levental, K. R. *et al.* Matrix crosslinking forces tumor progression by enhancing integrin signaling. *Cell* **139**, 891-906 (2009). https://doi.org:10.1016/j.cell.2009.10.027

185 Girton, T. S., Oegema, T. R. & Tranquillo, R. T. Exploiting glycation to stiffen and strengthen tissue equivalents for tissue engineering. *Journal of Biomedical Materials Research* **46**, 87-92 (1999). https://doi.org:10.1002/(sici)1097-4636(199907)46:1<87::Aid-jbm10>3.0.Co;2-k

186 Chaudhuri, O. *et al.* Extracellular matrix stiffness and composition jointly regulate the induction of malignant phenotypes in mammary epithelium. *Nat Mater* **13**, 970-978 (2014). https://doi.org:10.1038/nmat4009

187 Stowers, R. S., Allen, S. C. & Suggs, L. J. Dynamic phototuning of 3D hydrogel stiffness. *Proc Natl Acad Sci U S A* **112**, 1953-1958 (2015). https://doi.org:10.1073/pnas.1421897112

188 Wen, J. H. *et al.* Interplay of matrix stiffness and protein tethering in stem cell differentiation. *Nat Mater* **13**, 979-987 (2014). https://doi.org:10.1038/nmat4051

189 Trappmann, B. *et al.* Extracellular-matrix tethering regulates stem-cell fate. *Nat Mater* **11**, 642-649 (2012). https://doi.org:10.1038/nmat3339

190 Reinhart-King, C. A., Dembo, M. & Hammer, D. A. Endothelial Cell Traction Forces on RGD-Derivatized Polyacrylamide Substrata. *Langmuir* **19**, 1573-1579 (2002). https://doi.org:10.1021/la026142j

191 Forman, H. J., Zhang, H. & Rinna, A. Glutathione: overview of its protective roles, measurement, and biosynthesis. *Mol Aspects Med* **30**, 1-12 (2009). https://doi.org:10.1016/j.mam.2008.08.006

192 Singh, S. P., Schwartz, M. P., Lee, J. Y., Fairbanks, B. D. & Anseth, K. S. A peptide functionalized poly(ethylene glycol) (PEG) hydrogel for investigating the influence of biochemical and biophysical matrix properties on tumor cell migration. *Biomater Sci* **2**, 1024-1034 (2014). https://doi.org:10.1039/C4BM00022F

193 Quinlan, A. M. & Billiar, K. L. Investigating the role of substrate stiffness in the persistence of valvular interstitial cell activation. *J Biomed Mater Res A* **100**, 2474-2482 (2012). https://doi.org:10.1002/jbm.a.34162

194 Yao, T. & Asayama, Y. Animal-cell culture media: History, characteristics, and current issues. *Reprod Med Biol* **16**, 99-117 (2017). https://doi.org:10.1002/rmb2.12024

195 Hansen, J. N. Electrophoresis of ribonucleic acid on a polyacrylamide gel which contains disulfide cross-linkages. *Anal Biochem* **76**, 37-44 (1976). https://doi.org:10.1016/0003-2697(76)90261-x

196 Simic, R., Mandal, J., Zhang, K. & Spencer, N. D. Oxygen inhibition of free-radical polymerization is the dominant mechanism behind the "mold effect" on hydrogels. *Soft Matter* **17**, 6394-6403 (2021). https://doi.org:10.1039/d1sm00395j

197 Gandin, A. *et al.* Simple yet effective methods to probe hydrogel stiffness for mechanobiology. *Sci Rep-Uk* **11** (2021). https://doi.org:ARTN 22668
10.1038/s41598-021-01036-5

198 Yu, C. H. *et al.* Integrin-beta3 clusters recruit clathrin-mediated endocytic machinery in the absence of traction force. *Nat Commun* **6**, 8672 (2015). https://doi.org:10.1038/ncomms9672

199 Sladitschek-Martens, H. L. *et al.* YAP/TAZ activity in stromal cells prevents ageing by controlling cGAS-STING. *Nature* **607**, 790-798 (2022). https://doi.org:10.1038/s41586-022-04924-6

200 Kim, D. H., Chambliss, A. B. & Wirtz, D. The multi-faceted role of the actin cap in cellular mechanosensation and mechanotransduction. *Soft Matter* **9**, 5516-5523 (2013). https://doi.org:10.1039/C3SM50798J

201 Khatau, S. B. *et al.* A perinuclear actin cap regulates nuclear shape. *Proc Natl Acad Sci U S A* **106**, 19017-19022 (2009). https://doi.org:10.1073/pnas.0908686106

202 Kim, J. K. *et al.* Nuclear lamin A/C harnesses the perinuclear apical actin cables to protect nuclear morphology. *Nat Commun* **8**, 2123 (2017). https://doi.org:10.1038/s41467-017-02217-5

203 Maurer, M. & Lammerding, J. The Driving Force: Nuclear Mechanotransduction in Cellular Function, Fate, and Disease. *Annu Rev Biomed Eng* **21**, 443-468 (2019). https://doi.org:10.1146/annurev-bioeng-060418-052139

204 Lu, P., Takai, K., Weaver, V. M. & Werb, Z. Extracellular matrix degradation and remodeling in development and disease. *Cold Spring Harb Perspect Biol* **3** (2011). https://doi.org:10.1101/cshperspect.a005058

205 Wilson, M. J., Liliensiek, S. J., Murphy, C. J., Murphy, W. L. & Nealey, P. F. Hydrogels with well-defined peptide-hydrogel spacing and concentration: impact on epithelial cell behavior(). *Soft Matter* **8**, 390-398 (2012). https://doi.org:10.1039/C1SM06589K

206 Kamata, H., Kushiro, K., Takai, M., Chung, U. I. & Sakai, T. Non-Osmotic Hydrogels: A Rational Strategy for Safely Degradable Hydrogels. *Angew Chem Int Ed Engl* **55**, 9282-9286 (2016). https://doi.org:10.1002/anie.201602610

207 Armstrong, J. K., Wenby, R. B., Meiselman, H. J. & Fisher, T. C. The hydrodynamic radii of macromolecules and their effect on red blood cell aggregation. *Biophys J* **87**, 4259-4270 (2004). https://doi.org:10.1529/biophysj.104.047746

208 Masuelli, M. A. Dextrans in aqueous solution. Experimental review on intrinsic viscosity measurements and temperature effect. *Journal of Polymer and Biopolymer Physics Chemistry,* **1**, 13-21 (2013).